HHS Public Access

Author manuscript

Nature. Author manuscript; available in PMC 2017 June 13.

Published in final edited form as:

Nature. 2016 December 22; 540(7634): 583–587. doi:10.1038/nature20597.

NLRC3 is an inhibitory sensor of PI3K–mTOR pathways in cancer

Rajendra Karki[1,*], **Si Ming Man**[1,*], **R.K. Subbarao Malireddi**[1], **Sannula Kesavardhana**[1], **Qifan Zhu**[1,2], **Amanda R. Burton**[1], **Bhesh Raj Sharma**[1], **Xiaopeng Qi**[1], **Stephane Pelletier**[1,3], **Peter Vogel**[4], **Philip Rosenstiel**[5], and **Thirumala-Devi Kanneganti**[1]

[1]Department of Immunology, St. Jude Children's Research Hospital, Memphis, TN, 38105, USA

[2]Integrated Biomedical Sciences Program, University of Tennessee Health Science Center, Memphis, TN 38163, USA

[3]Embryonic Stem Cell Laboratory, St Jude Children's Research Hospital, Memphis, TN, 38105, USA

[4]Animal Resources Center and the Veterinary Pathology Core, St. Jude Children's Research Hospital, Memphis, TN, 38105, USA

[5]Institute of Clinical Molecular Biology, Christian-Albrechts-University Kiel, D-24105 Kiel, Germany

Abstract

Nucleotide-binding domain, leucine-rich repeat containing proteins (NLRs) belong to a large family of cytoplasmic sensors which regulate an extraordinarily diverse range of biological functions. NLRs contribute to immunity against infectious diseases, however, dysregulation of their functional activity leads to the development of inflammatory diseases and autoimmunity [1]. Cytoplasmic innate immune sensors, including NLRs, are central regulators of intestinal homeostasis [2–8]. NLRC3 (also known as CLR16.2 or NOD3) is a poorly characterized member of the NLR family and was identified in a genomic screen of genes encoding proteins bearing leucine-rich repeats (LRRs) and nucleotide-binding domains [9,10]. Expression of the gene encoding NLRC3 is drastically reduced in tumour tissues of patients with colorectal cancer compared with

Correspondence to: Thirumala-Devi Kanneganti, Department of Immunology, St. Jude Children's Research Hospital, MS #351, 262 Danny Thomas Place, Memphis TN 38105-3678, Tel: (901) 595-3634; Fax. (901) 595-5766. thirumala-devi.kanneganti@stjude.org.
*These authors contributed equally to this work.

Data Availability

Source data for Figures 3a, 3d, 3e, 3h, 4d–f, Extended data figures 3b, 5a, 6a, 6b, 6d, 6e, figure 9a, 9b, 9d–g, 10a and 10b have been provided in Supplementary Figure 1. All other data supporting the findings of this study are available from the corresponding author on request.

Competing financial interests

The authors declare no competing financial interests.

Authors Contributions

R.K., S.M.M., and T.D.K. conceptualized the study; R.K., S.M.M., R.K.S.M. and S.K. designed the methodology; R.K., S.M.M., R.K.S.M., S.K., Q.Z., B.R.S., A.R.B., X.Q., S.P. and P.V. performed the experiments; R.K., S.M.M., R.K.S.M., S.K., Q.Z., and P.V. conducted the analysis; R.K., S.M.M., and T.D.K. wrote the manuscript; P.R. and T.D.K. provided resources; T.D.K. provided overall supervision.

healthy tissues [11], highlighting an undefined potential function for this sensor in the development of cancer. Here, we found that mice lacking NLRC3 were hypersusceptible to colitis and colorectal tumorigenesis. The effect of NLRC3 was most dominant in enterocytes, where NLRC3 suppressed activation of the mTOR signalling pathways and inhibited cellular proliferation and stem-cell-derived organoid formation. NLRC3 associated with phosphoinositide 3-kinases (PI3Ks) and blocked activation of the PI3K–dependent kinase AKT following engagement of growth factor receptors or TLR4. These findings unveiled a key role for NLRC3 as an inhibitor of the mTOR pathways mediating protection against colorectal cancer.

Keywords

AKT; caspases; colorectal cancer; growth factors; immunity; inflammasomes; metabolism; NLRC3; mTOR; PI3K; proliferation; stem cells

---

Previous studies have shown that NLRC3 functions as a negative regulator of signalling pathways activated by Toll-like receptors (TLRs) and the DNA sensor STING in response to pathogen-associated molecular patterns or virus infection [12,13]. However, the physiological role of NLRC3 has remained largely unknown. We used an established mouse model of colitis-associated colorectal tumor igenesis to formally investigate the role of NLRC3 in colorectal cancer. Mice were injected intraperitoneally with azoxymethane (AOM), followed by three rounds of dextran sulfate sodium (DSS) treatment (Extended Data Fig. 1a). All time points referred to herein indicate the number of days after injection of AOM. The number of tumours was quantified 80 days after injection of AOM. Real-time qPCR analysis revealed a reduction in the expression of the gene encoding NLRC3 in tumour tissues compared with non-tumour-associated tissues in the colon of wild-type (WT) mice 80 days after injection of AOM (Extended Data Fig. 1b).

We treated cohorts of co-housed WT and *Nlrc3*$^{-/-}$ mice with AOM followed by three rounds of DSS and examined the prevalence of tumours in the colon of these mice 80 days after injection of AOM (Extended Data Fig. 1a, c). We found that *Nlrc3*$^{-/-}$ mice lost more body weight after the first two rounds of DSS and developed significantly more tumours compared with WT mice (Fig. 1a – d). Histological hallmarks associated with thickening of the colon, inflammation, ulceration, hyperplasia and the extent or severity of damage were more frequently identified in the middle and distal colon and the rectum of *Nlrc3*$^{-/-}$ mice compared with the corresponding regions in WT mice (Fig. 1e and f and Extended Data Fig. 1d). All of the *Nlrc3*$^{-/-}$ mice suffered high-grade dysplasia, whereas WT mice suffered low-grade dysplasia (Extended Data Fig. 1e). We found 63% of the *Nlrc3*$^{-/-}$ mice being positive for adenocarcinoma in the colon compared with 0% of the WT controls 80 days after injection of AOM (Extended Data Fig. 1f). Although NLRC3 showed a gene dose dependent response to AOM and DSS (Fig. 1g), it does not appear to have an effect on the normal mouse intestine or colon (Extended Data Fig. 1g).

Nlrc3$^{-/-}$ mice lost significantly more body weight and suffered more severe shortening of and damage to the colon after only single round of DSS treatment than their WT counterparts (Extended Data Fig. 2a – c). Certain members of the NLR family can form an inflammasome to drive maturation of IL-18, a cytokine important for mediating protection

against colitis-associated tumorigenesis [2–4,14]. We did not observe differential production of IL-18 in WT and *Nlrc3*$^{-/-}$ mice 14 and 80 days after injection of AOM (Extended Data Fig. 2d). Instead, production of the other inflammasome-associated cytokine IL-1β and inflammasome-independent cytokines IL-6, TNF and G-CSF and the chemokines KC (also known as CXCL1), MCP-1 (also known as CCL2) and MIP-1α (also known as CCL3) was elevated in colon tissues of *Nlrc3*$^{-/-}$ mice compared with WT mice 14 days after injection of AOM (Extended Data Fig. 2d – g). We further confirmed these results and found increased levels of circulating IL-6, G-CSF, KC and MIP-1α in the sera of *Nlrc3*$^{-/-}$ mice compared with WT mice 14 days after injection of AOM (Extended Data Fig. 2h). The expression of IL-17 and IL-22 was also elevated in the colon tissues of *Nlrc3*$^{-/-}$ mice compared with WT mice 14 days after injection of AOM, whereas the expression of IL-23, IFN-β and IFN-γ remained unchanged (Extended Data Fig. 3a). In agreement with the observation that *Nlrc3*$^{-/-}$ mice had elevated levels of many pro-inflammatory mediators 14 days after injection of AOM, we observed increased phosphorylation of IκBα and STAT3 in the colon tissues of *Nlrc3*$^{-/-}$ mice compared with WT mice (Extended Data Fig. 3b). However, differential phosphorylation of ERK was not observed (Extended Data Fig. 3b). Global increases in the production of inflammatory mediators and activation of immune signalling pathways reflected the hypersusceptibility of *Nlrc3*$^{-/-}$ mice to colitis.

We used flow cytometry to profile the immune cell populations in the colons of untreated WT and *Nlrc3*$^{-/-}$ mice (day 0) and WT and *Nlrc3*$^{-/-}$ mice 8 and 14 days after injection of AOM. We observed increased number of macrophages and NK cells in the colons of *Nlrc3*$^{-/-}$ mice compared with WT mice 14 days after AOM and DSS treatment (Extended Data Fig. 3c and d), which is consistent with the increased levels of inflammation observed at this time-point. However, we did not observe differences in the relative number of macrophages, CD11b^{+}CD11c^{+} cells, neutrophils, B cells, CD4^{+} T cells, CD8^{+} T cells and NK cells between untreated WT and *Nlrc3*$^{-/-}$ mice or between WT and *Nlrc3*$^{-/-}$ mice 8 days after injection of AOM (Extended Data Fig. 3d). NLRC3 has been implicated in the regulation of T cell activation [10], however, we did not observe a difference in the levels of IFN-γ^{+} or TNF^{+} CD4^{+} T cells when WT and *Nlrc3*$^{-/-}$ splenocytes were stimulated with CD3 and CD28 in the presence of IL-2 (Extended Data Fig. 3e).

We performed bone-marrow chimera studies to identify the contribution of NLRC3 in haematopoietic cells versus radio-resistant stromal cells during colitis-associated tumorigenesis. As expected, *Nlrc3*$^{-/-}$ mice which received *Nlrc3*$^{-/-}$ bone marrow were more susceptible to tumorigenesis compared with WT mice which received WT bone marrow (Fig. 1h and Extended Data Fig. 4a). However, *Nlrc3*$^{-/-}$ mice which received WT bone marrow had significantly increased tumour burden compared with WT mice which received WT bone marrow. In addition, WT mice which received *Nlrc3*$^{-/-}$ bone marrow had significantly increased tumour burden compared with WT mice which received WT bone marrow (Fig. 1h and Extended Data Fig. 4a). We further confirmed our findings and generated mice lacking NLRC3 specifically in haematopoietic cells (Vav1^{Cre}*Nlrc3*$^{fl/fl}$), cells of the myeloid lineage (LysM^{Cre}*Nlrc3*$^{fl/fl}$), and intestinal epithelial cells (Vil^{Cre}*Nlrc3*$^{fl/fl}$). Mice lacking NLRC3 in intestinal epithelial cells developed the highest number of tumours, followed by mice lacking NLRC3 in haematopoietic cells (Fig. 1i and Extended Data Fig. 4b). Mice lacking NLRC3 in cells of the myeloid lineage had a similar number of tumours

compared with WT mice (Fig. 1i and Extended Data Fig. 4b). These data supported the observation that the inhibitory effect of NLRC3 is more dominant in intestinal epithelial cells, whereas its effect is more subtle in haematopoietic cells.

A closer examination of intestinal epithelial cells of *Nlrc3*$^{-/-}$ mice revealed significantly increased numbers of both Ki67^{+} and PCNA^{+} cells per intestinal crypt compared with WT mice 14 days after injection of AOM (Fig. 2a). In addition, colonic epithelial stem cells harvested from *Nlrc3*$^{-/-}$ mice more readily developed into organoids in *ex vivo* culture compared with those harvested from WT mice (Fig. 2b). The average diameters of the organoids derived from *Nlrc3*$^{-/-}$ mice were significantly increased compared with the average diameters of the organoids from WT mice (Fig. 2b). Expression of the gene encoding the stem cell marker LGR5 in the colon tissues was similar between WT and *Nlrc3*$^{-/-}$ mice (Extended Data Fig. 4c), suggesting that the differences in the number and size of intestinal organoids was because of differential colony-forming capacity rather than differences in the numbers of starting intestinal stem cells. To more directly investigate the effect of NLRC3 on cell proliferation, we overexpressed NLRC3 in the human colon cell line HCT116 and found reduced proliferation in these cells compared with cells expressing a control GFP protein (Fig. 2c). Furthermore, primary *Nlrc3*$^{-/-}$ fibroblasts proliferated more rapidly than did WT fibroblasts (Fig. 2d).

Cellular proliferation can also be achieved when growth factors, nutrients and cellular energy activate metabolic pathways via the kinase known as mammalian target of rapamycin (mTOR) [15]. We found increased phosphorylation of the mTOR downstream targets S6, 4E–BP1 and AKT at S473 in the colon tissues of *Nlrc3*$^{-/-}$ mice compared with WT mice 14 days after injection of AOM (Fig. 3a, b). Increased phosphorylation of these mTOR targets was also observed in *Nlrc3*$^{-/-}$ organoids compared with WT organoids (Fig. 3c, d). However, we found no difference in the expression of genes encoding the Wnt signalling pathway, including WNT, β-catenin, LEF1, TCF4, TCF7 and AXIN-2 in colon tissues between WT and *Nlrc3*$^{-/-}$ mice prior to treatment or 14 days after injection of AOM (Extended Data Fig. 4c). The extent of nuclear localisation of β-catenin was also similar between WT and *Nlrc3*$^{-/-}$ mice (Extended Data Fig. 4d).

Dysregulation of the mTOR signalling pathways in *Nlrc3*$^{-/-}$ mice occurred very early – 8 days after injection of AOM, whereas no difference in the production of inflammatory cytokines and mediators and phosphorylation of IκBα was observed at this time-point (Extended Data Fig. 5, a–c). In addition, the differential AKT-mTOR signalling at this time point was not caused by differences in the relative levels of immune cells recruited to the colon (Extended Data Fig. 3d). These data suggested that dysregulated mTOR signalling observed at an earlier time point may lead to increased NF-κB signalling at a later time point.

Phosphorylation and activation of mTOR is driven by a number of upstream signalling proteins in the PI3K–AKT–mTOR pathway. Phosphorylation of AKT at the T308 site by the kinase PDK1 licenses the ability of AKT to activate mTOR [16–18]. To examine whether NLRC3 directly affects the apical molecules in the PI3K–AKT–mTOR pathway, we first investigated the phosphorylation status of AKT at the T308 site. We observed elevated

phosphorylation of AKT at the T308 site in the colon tissues of *Nlrc3*$^{-/-}$ mice compared with WT mice 14 days after injection of AOM (Fig. 3e). Increased phosphorylation of AKT in colon tissues was found predominately in epithelial cells, and to a lesser extent, in infiltrating cells (Fig. 3f). Similarly, increased phosphorylation of AKT at T308 was observed in *Nlrc3*$^{-/-}$ organoids treated with IGF-1 compared with WT controls (Fig. 3g, h). We further observed increased activation of PDK1 in the colon tissues of *Nlrc3*$^{-/-}$ mice treated with AOM and DSS compared with WT mice (Fig. 3e). In addition, the elevated phosphorylation of AKT at T308 and of 4E–BP1 were found in the colon of *Nlrc3*$^{+/-}$ heterozygote mice compared with littermate WT mice 14 days after injection of AOM, albeit not as elevated as that observed in littermate *Nlrc3*$^{-/-}$ mice (Extended Data Fig. 6a). The gene-dose-dependent effect of NLRC3 on the suppression of the mTOR signalling pathways was largely reminiscent of the gene-dose-dependent effect of NLRC3 on the suppression of tumorigenesis (Fig. 1g).

Activated mTOR is phosphorylated and migrates to lysosomal and late endosomal membranes [19,20]. Indeed, we observed increased phosphorylation of mTOR in the colon tissues of *Nlrc3*$^{-/-}$ mice (Fig. 3e). We also found an increased co-localisation frequency between mTOR and LAMP1 puncta in IGF-1-treated primary *Nlrc3*$^{-/-}$ fibroblasts compared with untreated primary WT fibroblasts (Fig. 4a). Increased mTOR signalling was observed in *Nlrc3*$^{-/-}$ fibroblasts or WT fibroblasts treated with si-RNAs against the gene encoding NLRC3 compared with their corresponding controls (Extended Data Fig. 6b – e and Fig. 7, a–d).

We further investigated whether NLRC3 can restrict proliferation in a spontaneous mouse model of colon cancer. We crossed the mouse line containing a heterozygous mutation in the gene encoding adenomatous polyposis coli (*Apc*$^{Min/+}$) with *Nlrc3*$^{-/-}$ mice and found that *Apc*$^{Min/+}$ *Nlrc3*$^{-/-}$ mice had a higher tumour burden than *Apc*$^{Min/+}$ control mice (Extended Data Fig. 8a). 40% of the *Apc*$^{Min/+}$ *Nlrc3*$^{-/-}$ mice developed hyperplasia compared with none in the littermate control group and that *Apc*$^{Min/+}$ *Nlrc3*$^{-/-}$ mice had increased damage in the colon (Extended Data Fig. 8b, c). Importantly, we observed increased number of Ki67^{+} proliferative cells and cells positive for phosphorylated S6 in the colon of *Apc*$^{Min/+}$ *Nlrc3*$^{-/-}$ mice compared with *Apc* $^{Min/+}$ mice (Extended Data Fig. 8c). Further, *Apc*$^{Min/+}$ *Nlrc3*$^{-/-}$ intestinal stem cells had a greater capacity to proliferate into organoids compared with that of *Apc*$^{Min/+}$ intestinal stem cells (Extended Data Fig. 8d). Treatment with the phosphatidylinositol 3-Kinase (PI3K) inhibitor LY294002 and mTOR inhibitor rapamycin impaired the ability of intestinal stem cells to proliferate into organoids (Extended Data Fig. 8d). Treatment of the *Apc*$^{Min/+}$ mice and *Apc*$^{Min/+}$ *Nlrc3*$^{-/-}$ mice with the PI3K–mTOR inhibitor NVP-BEZ235 reduced the tumour burden and phosphorylation of S6 in the tumors and enterocytes of *Apc*$^{Min/+}$ *Nlrc3*$^{-/-}$ mice to a level observed in treated *Apc*$^{Min/+}$ mice (Fig. 4b and c). Collectively, these data suggested that NLRC3 restricts proliferation via the PI3K–mTOR axis during colon tumorigenesis.

Following generation of inositol phospholipids by activated Class IA PI3Ks, AKT is recruited to the cell membrane where it undergoes a conformational change and phosphorylation at T308 by PDK1 [16–18]. Co-immunoprecipitation assays showed that NLRC3 weakly interacted with PDK1 and did not interact with AKT (Fig. 4d). Instead, we

found NLRC3 co-immunoprecipitated with p85 subunits of Class IA PI3Ks (Fig. 4d). In addition, we found increased interaction between the p85 and p110α subunits of PI3K in *Nlrc3*$^{-/-}$ primary fibroblasts or mouse bone marrow-derived macrophages (BMDMs) (Extended Data Fig. 9a,b). We also found a higher level of phosphorylation and activation of p85 PI3K in the colon tissues of *Nlrc3*$^{-/-}$ mice treated with AOM-DSS compared with WT mice (Fig. 4e). These data provided evidence to suggest that NLRC3 disrupted an association between the PI3K p85 and p110α subunits and reduced the activity of PI3K p85 itself. Deletion of the CARD, NACHT or LRR domain of NLRC3 impaired the ability of NLRC3 to interact with either the PI3K p85 or p110α subunit (Extended Data Fig. 9, c–g). Reconstitution of NLRC3 in *Nlrc3*$^{-/-}$ fibroblasts reduced phosphorylation of AKT T308 and other downstream molecules to levels similar to that found in WT fibroblasts upon stimulation with IGF-1 (Fig. 4f).

In addition to growth factor receptors, activation of TLR4 can engage the PI3K–AKT–mTOR pathway [21–23]. Indeed, we found a increased activation of the mTOR signalling pathways in LPS-treated primary *Nlrc3*$^{-/-}$ BMDMs compared with LPS-treated WT BMDMs (Extended Data Fig. 10a,b). We further confirmed our findings in an independently generated line of NLRC3-deficient mice, called *Nlrc3*$^{ld/ld}$ mice (NLRC3 large deletion, data not shown, see Methods section). These findings collectively unveiled NLRC3 as an inhibitory sensor of the PI3K–AKT–mTOR pathway mediating protection against tumorigenesis in colorectal cancer (Extended Data Fig. 10c).

The biological importance of NLRC3 in the host is not confined to cancer and infectious diseases. A previous study has shown that expression of NLRC3 is down-regulated in patients with the autoimmune disease Wegener's granulomatosis [24]. Moreover, a loss-of-function mutation in the gene encoding the NLRC3-like protein in zebrafish results in systemic inflammation [25]. These findings collectively provide evidence to support a cross-species functionality of NLRC3. Whether NLRC3 requires binding to a specific ligand or that NLRC3 is engaged in a ligand-independent manner in the activation of its regulatory function remains to be explored. Understanding the precise functions of NLRC3 could open up new avenues for the treatment of infectious disease, autoinflammation and cancer.

Methods

Mice

WT (C57BL/6) and *Nlrc3*$^{-/-}$ mice were bred and maintained under specific pathogen-free conditions at St. Jude Children's Research Hospital, USA. To generate the *Nlrc3*$^{-/-}$ mice, exons 2 and 3 of the gene encoding NLRC3 (2.5 kb) were excised, which resulted in deletion of 661 amino acids encoding the N-terminal caspase recruitment domain (also known as CARD) and the central nucleotide-binding domain (also known as NACHT) of NLRC3. Splicing of exon 1 and exon 4 led to a frameshift, generating a premature stop codon (Extended Data Fig. 1c). The targeting vector ROS1-HR was linearized and transfected into embryonic stem (ES) cells. Cells positive for the targeting vector were selected by their resistance to 200 μg/ml of G418 and further screened for 5' and 3' homologous recombination. ES cell clones with the correct targeting events were used for blastocysts injection. CMV-Cre mice were used to delete the conditional *Nlrc3*-floxed allele

to generate the *Nlrc3*$^{-/-}$ mice. B6.129P2-*Lyz2*$^{tm1(cre)Ifo}$/J (004781, The Jackson Laboratory), B6.Cg-Tg(Vav1-icre)A2Kio/J (008610, The Jackson Laboratory) and B6.Cg-Tg(Vil-cre)997Gum/J mice (004586, The Jackson Laboratory) were used to delete the conditional *Nlrc3*-floxed allele in a cell-type-specific manner. Expression of NLRC3 in WT and *Nlrc3*$^{-/-}$ mice were confirmed by genomic PCR amplification (Extended Data Fig. 1c). *Nlrc3*$^{-/-}$ mice were backcrossed to C57BL/6 for 9 generations.

Nlrc3$^{ld/ld}$ (NLRC3 large deletion) mice were generated by injection of 2 single guide RNAs (Nlrc3-Guide-01: ATTCCCAGGTCGTCTTAGGC [125 ng/μl] and Nlrc3-Guide-02: AGTGGAACAGCACAGTTCGC [125 ng/μl]), designed to introduce DNA double-strand breaks into intron 1 and intron 3 of the *Nlrc3* gene, together with a codon optimized Cas9 mRNA transcript (50 ng/μl) into the cytoplasm of the pronuclear stage C57BL/6J zygotes (Transgenic Core Unit, St. Jude Children's Research Hospital). Injected embryos were surgically transplanted into oviducts of pseudo pregnant CD1 females and newborn mice bearing the intron 1 to intron 3 deletion (~3.8kb) were identified by the amplification of a 1.1 kb fragment using primers flanking the 2 break sites: Nlrc3-F51: AGAGTGGTGCCATCTTCTGC and Nlrc3-R32: CTCAAGTCAGGGCAGCATGA. Sanger sequencing of the ~1.1 kp amplicon confirmed proper deletion of the 3.8 kb fragment containing exon 2 and 3. The sgRNAs and Cas9 mRNA transcript were designed and generated as described previously [26]. Potential off-target sites were identified using Cas-OFFinder [27], amplified by PCR and sequenced. No off-target site cleavage was observed. Two founder mice were used to establish the mouse lines. Animal study protocols were approved by the St. Jude Children's Research Hospital Committee on Use and Care of Animals.

AOM-DSS model of colorectal tumorigenesis

Male and female mice were used at the age of six weeks. For cohousing experiments, WT and *Nlrc3*$^{-/-}$ mice were co-housed for three weeks and separated prior to injection of AOM. We also performed experiments whereby WT and *Nlrc3*$^{-/-}$ mice were co-housed for three weeks prior to injection of AOM and were remained co-housed over the course of the experiments. In both cases, the results did not differ. Mice were injected intraperitoneally with 10 mg of AOM (A5486, Sigma) per kg body weight according to previously established protocols [7,28]. Five days later, 2% DSS (9011-18-1, Affymetrix eBioscience) was given in the drinking water for 6 days followed by regular drinking water for 2 weeks. This cycle was repeated twice with 1.5% DSS and mice were sacrificed on Day 80 (Extended Data Fig. 1a). For Day 8 samples, mice were injected with AOM, and after 5 days, fed with 2% DSS for 3 days before mice were harvested. For Day 14 samples, mice were injected with AOM, and after 5 days, fed with 2% DSS for 6 days. Mice were then fed with regular water for 3 days and harvested. Bone-marrow chimera studies were performed as described previously [7]. No randomization or blinding was performed.

Apc^{Min} model of colorectal tumorigenesis

C57BL/6J–*Apc*$^{Min/+}$/J mice (002020, The Jackson Laboratory) were used to crossed with *Nlrc3*$^{-/-}$ mice. Littermate *Apc*$^{Min/+}$ and *Apc*$^{Min/+}$ *Nlrc3*$^{-/-}$ mice were administered with either 40 mg/kg body weight of the dual inhibitor of PI3K and mTOR, NVP-BEZ235

(N-4288, LC Laboratories) dissolved in 10% 1-Methyl-2-pyrrolidone (328634, Sigma) plus 90% v/v polyethylene glycol 300 (90878, Sigma) or the control vehicle 10% v/v 1-Methyl-2-pyrrolidone plus 90% v/v polyethylene glycol 300 by daily oral gavage for 40 days from 6 weeks of age.

Histology and microscopy analysis

Colons were rolled into a "Swiss roll" and fixed in 10% formalin, processed and embedded in paraffin by standard techniques. Longitudinal sections of 5 μm thick were stained with hematoxylin and eosin (H&E) and examined by a pathologist blinded to the experimental groups. Colitis scores were assigned based on inflammation, ulceration, hyperplasia and the extent or severity of damage. Severity scores for inflammation were assigned as follows: 0 = normal (within normal limits); 2 = minimal (mixed inflammation, small, focal or widely separated, limited to lamina propria); 15 = mild (multifocal mixed inflammation, often extending into submucosa); 40 = moderate (large multifocal lesions within mixed inflammation involving mucosa and submucosa); 80 = marked (extensive mixed inflammation with edema and erosions; 100 = severe (diffuse inflammation with transmural lesions and multiple ulcers). Scores for ulceration were assigned as follows: 0 = normal (none); 2 = minimal (only one small focus of ulceration involving fewer than 5 crypts); 15 = mild (a few small ulcers up to 5 crypts); 40 = moderate (multifocal ulcers up to 10 crypts; 80 = marked (multifocal to coalescing ulcers involving more than 10 crypts each); 100 = severe (extensive to diffuse with multiple ulcers covering more than 20 crypts each). Scores of hyperplasia were assigned as follows: 0 = normal; 2 = minimal (some areas with crypts elongated and increased mitoses); 15 = mild (multifocal areas with crypts elongated up to twice the normal thickness, normal goblet cells present); 40 = moderate (extensive areas with crypts up to 2 times the normal thickness, reduced goblet cells); 80 = marked (mucosa over twice the normal thickness, hyperchromatic epithelium, reduced or rare goblet cells, possibly foci of arborization); 100 = severe (mucosa twice the normal thickness, marked hyperchromasia, crowding or stacking, absence of goblet cells, high mitotic index and arborization). Scores of extent were assigned as follows: 0 = normal (rare or inconspicuous lesions); 2 = minimal (less than 5% involvement); 15 = mild (multifocal but conspicuous lesions, 5 to 10% involvement); 40 = moderate (multifocal, prominent lesions, 10 to 50% involvement); 80 = marked (coalescing to extensive lesions or areas of inflammation with some loss of structure, 50 to 90% involvement); 100 = severe (diffuse lesion with effacement of normal structure, over 90% involvement). The proliferating cells in the intestinal epithelium were detected by immunoperoxidase staining for Ki67 and PCNA. The immunohistochemistry antibodies used were: Ki67 (NBP1–40684, Novus), PCNA (M0879, DAKO), β-catenin (610154, BD), P-AKT Ser473 (4060, Cell Signalling), and P-S6 Ribosomal Protein Ser235–236 (4858, Cell Signalling). Tissues were counterstained with haematoxylin. The number of $Ki67^+$ or $PCNA^+$ cells per crypt in each animal was counted (at least 18–20 crypts per mouse).

Cell culture and stimulation of cells

Pinna of adult WT and *Nlrc3*$^{-/-}$ mice were minced and digested with 100 mg/ml collagenase type IV (LS004188, Worthlington Biochemical Corporation) for 3 h, followed by filtration through 70-μm strainers to obtain fibroblasts. Cells were cultured in 50% FBS (TMS-013-B,

Millipore) in DMEM (11995073, ThermoFisher Scientific) supplemented with HEPES (15630-080, ThermoFisher Scientific), 1% penicillin and streptomycin (15070-063, ThermoFisher Scientific), L-glutamine (25030, ThermoFisher Scientific), sodium pyruvate (11360, ThermoFisher Scientific), non-essential amino acids (11140, ThermoFisher Scientific), and β-mercaptoethanol (21985023, ThermoFisher Scientific) for the first 3–4 days. Cells were subcultured in 10% FBS in DMEM supplemented with 1% penicillin and streptomycin. All primary fibroblasts were used before reaching the sixth passage. Fibroblasts were seeded onto six-well plates at a density of 2×10^5 cells per well. Cells were deprived of serum for 36 h and further incubated in PBS for 1 h. Cells were then stimulated with 50 ng/ml of recombinant murine IGF-1 (250-19, Peprotech) for the indicated time.

Primary mouse bone marrow-derived macrophages (BMDMs) were cultured as described previously [29]. BMDMs were stimulated with 500 ng/ml ultrapure LPS from *Salmonella minnesota* R595 (tlrl-smlps, InvivoGen) for the indicated time. The human colorectal carcinoma HCT116 cell line (ATCC#CCL-247, American Type Culture Collection) was cultured in McCoy's 5A media (16600-082, ThermoFisher Scientific) supplemented with 10% FBS and 1% penicillin and streptomycin. The embryonic kidney epithelial cell line HEK293T (ATCC#3216, American Type Culture Collection) and L929 cell line (ATCC#CRL-2648, American Type Culture Collection) were cultured in DMEM supplemented with 10% FBS. All cell lines were maintained at 37°C with 5% CO_2.

Colon organoid culture

Mouse colon stem cells were cultured using IntestiCult Organoid Growth Media according to the manufacturer's instructions (06005, STEMCELL Technologies). The whole colon was removed from untreated WT and *Nlrc3*$^{-/-}$ mice and rinsed with cold PBS. The colon was cut into 2 mm segments and washed 20 times with cold PBS. Colonic segments were incubated in Gentle Cell Dissociation Reagent (07174, STEMCELL Technologies), rotated at 350 g for 15 min at room temperature, followed by resuspension in 0.1% BSA (A6003, Sigma) in PBS. Dissociated colonic crypts were filtered through 70-μm strainers. Dissociated colonic crypts were resuspended in DMEM/F12 medium with 15 mM HEPES (36254, STEMCELL Technologies), counted and resuspended in Intesticult Organoid Growth Media and Matrigel (356230, Corning) in a 1:1 ratio. Cells were plated in 24-well culture plates (3738, Corning). Intesticult Organoid Growth Media were added to the cell culture plates to immerse the matrix composed of Intesticult Organoid Growth Media and Matrigel. For inhibition studies, 50 μM of LY294002 (440202, Millipore) or 10 μg/ml rapamycin (553210, Sigma) was added to the Intesticult Organoid Growth Media.

Proliferation Assay

Cell proliferation was measured using the WST-1 reagent (05015944001, Roche). Primary ear fibroblasts or HCT116 cells were plated at a density of 5,000 cells per well in 96-well tissue culture plates and incubated overnight. Cells were deprived of serum for 36 h and exposed to normal culture media for the indicated time interval. The WST-1 reagent was added to the cells for 2 h. Plates were then read at 450 nm. The number of cells was calculated using a standard curve [30].

Immunoblotting

Proteins were extracted from colon tissues or cells using RIPA lysis buffer supplemented with protease (11697498001, Roche) and phosphatase inhibitors (04906837001, Roche) as described previously [31]. Samples were resolved in 8–15% SDS-PAGE and transferred onto PVDF membranes (IPVH00010, Millipore). Blocking was performed in 5% milk for 1 h and membranes were incubated in primary antibodies overnight at 4°C. Membranes were incubated with HRP-conjugated secondary antibody for 1 h and proteins were visualized using Super Signal Femto substrate (34096, ThermoFisher Scientific). The primary antibodies used were P-ERK (1:1,000, 9101, Cell Signalling), ERK (1:1,000, 9102, Cell Signalling), P-IκBα (1:1,000, 9241, Cell Signalling), IκBα (1:1,000, 9242, Cell Signalling), P-AKT Ser473 (1:1,000, 4060, Cell Signalling), P-AKT Thr308 (1:1,000, 13038); AKT (1:1,000, 4691, Cell Signalling), P-mTOR Ser2448 (1:1,000, 2971, Cell Signalling), mTOR (1:1,000, 2972, Cell Signalling), P-p70 S6K Thr389 (1:1,000, 9205, Cell Signalling), P-S6 Ser235/236 (1:1,000, 4856, Cell Signalling), P-4E–BP1 Thr37/46 (1:1,000, 2855, Cell Signalling), P-STAT3 Tyr705 (1:1,000, 9131, Cell Signalling), P-PDK1 (1:1,000, 3061, Cell Signalling), PDK1 (1:1,000, 3062, Cell Signalling), P-PI3K p85 (1:1,000, 4228, Cell Signalling), PI3K p85 (1:1,000, 4257, Cell Signalling), PI3K p110α (1:1,000, 4249, Cell Signalling), mouse anti-GFP (1:2,000, sc-9996, Santa Cruz Biotechnology), rabbit anti-GFP (1:2,000, sc-8334, Santa Cruz Biotechnology), β-actin (1:2,000, 8457, Cell Signalling), and anti-GAPDH (1:10,000; 5174, Cell Signalling). Immunoblots were quantified using ImageJ.

Immunofluorescence staining

Serum deprived primary ear fibroblasts were left untreated or stimulated with IGF-1 for 30 minutes. Fibroblasts or six-day-old intestinal organoids were washed three times with PBS and were fixed for 15 min at room temperature in 4% paraformaldehyde, followed by blocking in 10% normal goat serum (X090710-8, Dako) supplemented with 0.1% saponin (47036, Sigma). Fibroblasts or organoids were incubated with the following antibodies overnight at 4°C: P-AKT S473 (1:200, 4060, Cell Signalling), P-AKT T308 (1:200, 13038); P-S6 Ser235/236 (1:500, 4856, Cell Signalling), P-4E–BP1 T37/46 (1:200, 2855, Cell Signalling). Samples were also stained with Alexa Fluor 488 Phalloidin (1:500, A12379, ThermoFisher Scientific) or Alexa Fluor 488 E-cadherin (1:200, 53–3249-80, Affymetrix eBioscience). To analyze mTOR activation, cells were incubated overnight at 4°C with antibodies against mTOR (1:200, 2983, Cell Signalling) and LAMP1 (1:1,000, eBio1D4B, Affymetrix eBioscience). The secondary antibodies used were Alexa Fluor 568-conjugated antibody to rabbit immunoglobulin G (1:250; A11036; ThermoFisher Scientific), Alexa Fluor 568-conjugated antibody to rat immunoglobulin G (1:250; A11077; ThermoFisher Scientific) and Alexa Fluor 488-conjugated antibody to rabbit immunoglobulin G (1:250; A11034; ThermoFisher Scientific). Cells and organoids were counterstained in DAPI mounting medium (H-1200, Vecta Labs) and images taken with a Nikon C2 confocal microscope. The average density unit and the Pearson’s correlation coefficient were calculated using the digital microscopy imaging software SlideBook 5 (Intelligent Imaging Innovations).

Real time qRT-PCR

RNA was isolated using Trizol (15596026, ThermoFisher Scientific) and converted to cDNA using the High capacity cDNA Reverse Transcription kit (4368814, Applied Biosystems). Gene expression was assessed using the 2× Sybrgreen kit (4368706, Applied Biosystems) according to the manufacturer's instructions. Sequences for qRT-PCR primers are listed in Supplementary Information.

Cytokine measurement by ELISA

Cytokines in the colon and sera were measured by ELISA according to manufacturers' instructions. IL-18 was measured using an ELISA kit (BMS618/3TEN, Affymetrix eBioscience) and all other cytokines were measured by a multiplex ELISAs (MCYTOMAG-70K, Millipore).

Flow cytometry

Colons were dissected, washed with ice-cold PBS and cut into small pieces. Colons pieces were incubated with PBS containing 1 mM DTT, 5 mM EDTA and 10 mM HEPES at 37°C for 30 min with gentle shaking to remove the epithelial layer. The colon segments were further digested in RPMI medium containing 0.5 mg/ml collagenase D at 37°C for 1.5 hr. The supernatant was passed through 70 μm cell strainer and enriched by 37.5% Percoll to isolate lamina propria cells.

The following monoclonal antibodies were used for flow cytometry: CD4 (RM4–5; 14–0042–85), CD11b (M1/70; 48–0112-82) and CD8a (53-6.7; 48–0081–82) from Affymetrix eBioscience, CD19 (6D5; 115512), NK1.1 (PK136; 108708), CD11c (N418; 117306), Gr1 (RB6–8C5; 108426) and F4/80 (BM8; 123109) from BioLegend. The dilution factor for all antibodies was 1:300. The following gating strategies were used: B cells were gated as live cells and $CD19^+$. $CD4^+$ T cells were gated as live cells, $CD4^+$ and $CD8^-$. $CD8^+$ T cells were gated as live cells, $CD8^+$ and $CD4^-$. NK cells were gated as live cells and $NK1.1^+$. Macrophages were gated as live cells, $CD11b^+$, $Gr1^{low\text{-}neg,}$ $F4/80^+$ and $CD11c^-$. Neutrophils were gated as live cells, $CD11b^+$ and $Gr1^{hi}$. $CD11b^+CD11c^+$ cells were gated as live cells, $CD11b^+$, $Gr1^{low\text{-}neg,}$ $CD11c^+$ and $F4/80^-$. Flow cytometry data were acquired on a BD FACSCalibur and analysed using TreeStar FlowJo software.

T cell stimulation and intracellular cytokine staining

Splenocytes from WT and *Nlrc3*$^{-/-}$ mice were treated with ACK lysis buffer at room temperature for 1 min to remove red blood cells. Splenocytes were washed, counted and plated at 2×10^5 cells per well in a 96-well plate coated with 1 μg/mL anti-CD3 (145-2C11, Affymetrix eBioscience) and 1 μg/mL anti-CD28 (16–0281, Affymetrix eBioscience). Cells were cultured at 37°C with and without 20 ng/ml murine IL-2 (212-12, Peprotech) for 4 days. Brefeldin A (00–4506, Affymetrix eBioscience) was added to the media for 3 h, followed by washing in PBS, and staining with anti-CD4 (14–0042–85, Affymetrix eBioscience) and anti-CD3 (145-2C11, Affymetrix eBioscience) antibodies on ice for 20 min. Stained cells were fixed in 1% paraformaldehyde for 30 min on ice and permeabilized using permeabilization buffer (00–8333-56, Affymetrix eBioscience) according to manufacturer's instructions. To detect intracellular cytokines, fixed cells were stained with

anti-IFN-γ (50–7311, Tonbo) and anti-TNF (506322, Biolegend) for 30 min on ice. Flow cytometry were performed as described above.

Small interfering RNA knockdown

Primary ear fibroblasts were transfected with a small interfering RNA (siRNA) from siGENOME smart pools with the assistance of the Neon Transfection System (MPK5000, ThermoFisher Scientific). The siGENOME SMARTpool siRNA specific for the gene encoding mouse NLRC3 (M-052823-01, Dharmacon) and a control siRNA pool were used. Sequences for siRNA are listed in Supplementary Information. After 48 h of transfection, cells were stimulated with IGF-1 as described above.

Retroviral transduction

Human or mouse MSCV-NLRC3-IRES-GFP or MSCV-IRES-GFP was co-transfected with a retroviral packaging plasmids (pPAM-E and VSV-G) into HEK293T cells using Xfect Transfection Reagents (631318, Clontech Laboratories, Inc.). Virus-containing media were collected 48–72 h later and passed through a 45-μm filter. Primary ear fibroblasts or HCT116 cells were transduced with control or NLRC3-encoding retroviral vectors. Cells expressing GFP were selected by flow cytometry.

Generation of cells expressing NLRC3 and its deletion mutants

Plasmids pVSVg, pEQ-Pam3(−E) and pMIGII encoding the mouse *Nlrc3* gene and deletion mutants were transfected into L929 cells to generate retroviral stocks. Domains were annotated in accordance to the NCBI Conserved Domain (http://www.ncbi.nlm.nih.gov/Structure/cdd/wrpsb.cgi). Retroviral supernatants were harvested after 48 h of transfection and filtered through 0.4 μm filters. L929 cells were infected with the retroviral stocks in the presence of polybrene to generate cells stably expressing either WT NLRC3 or NLRC3 deletion mutant proteins.

Co-immunoprecipitation

Cells were collected with ice-cold PBS and lysed in lysis buffer composed of 50 mM Tris-HCl pH 7.5, 150 mM NaCl, 1% NP-40, protease and phosphatase inhibitors. Lysates were cleared of insoluble material by centrifugation at 15,000 g for 10 min. For immunoprecipitation, cell lysates were incubated with 3 μg of primary antibodies at 4 °C for 12–16 h on a rocking platform, followed by incubation with Protein A/G PLUS-Agarose (sc-2003, Santa Cruz) for a further 2 h on a rocking platform. The immunoprecipitated products were washed three times with lysis buffer and eluted using 2× SDS sample buffer and boiled at 100 °C for 5 min.

Statistical analysis

GraphPad Prism 6.0 software was used for data analysis. Data are shown as mean ± s.e.m. Statistical significance was determined by *t* tests (two-tailed) for two groups or One-way ANOVA (with multiple comparisons tests) for three or more groups. $P<0.05$ was considered statistically significant.

Extended Data

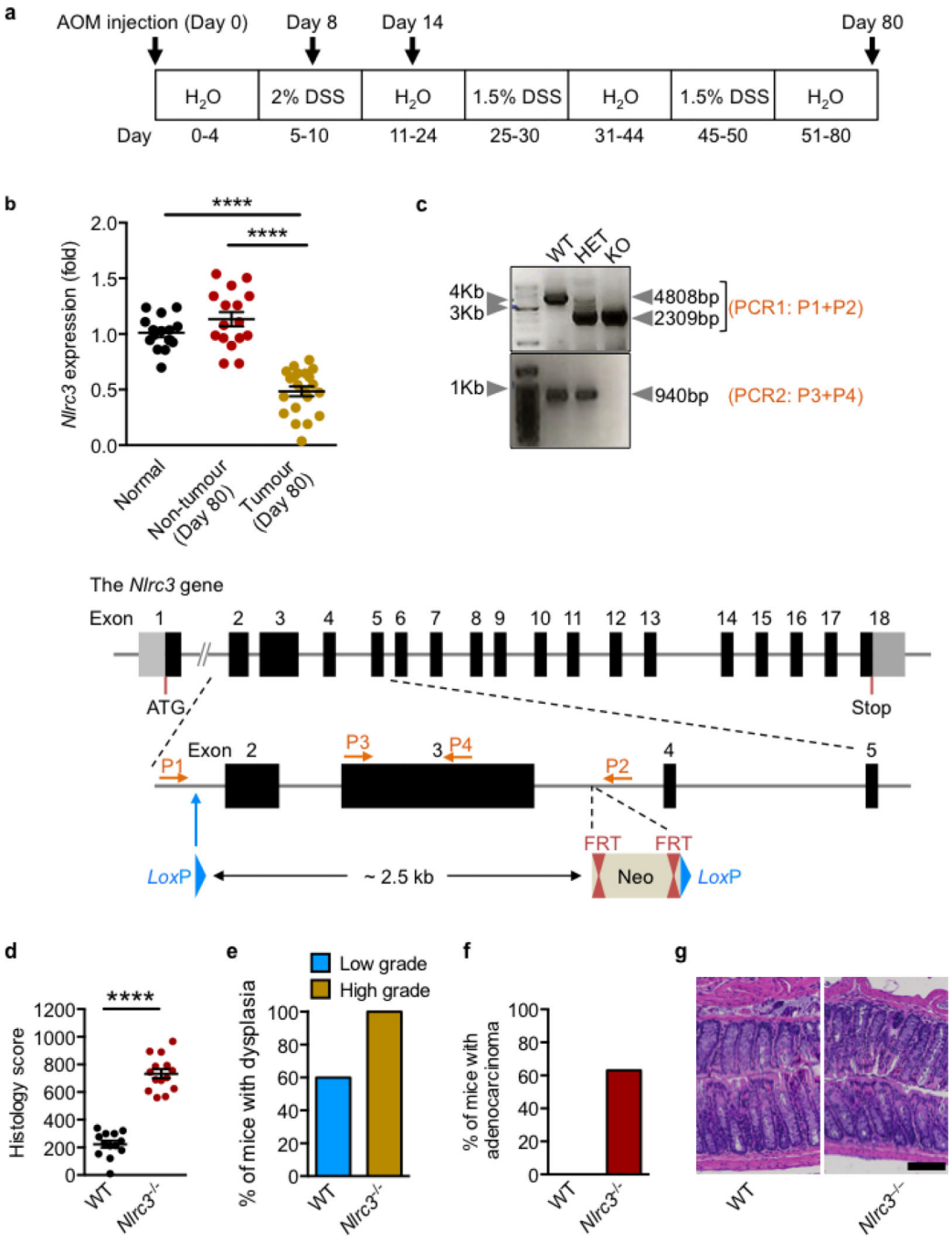

Extended Data Figure 1. NLRC3 prevents colitis-associated colorectal tumorigenesis

a, Timeline for azoxymethane (AOM) and dextran sulfate sodium (DSS) treatment. **b**, Relative expression of the gene encoding NLRC3 in tumour and non-tumour tissues in the colon of WT mice 80 days after AOM injection. **c**, Targeting strategy used to generate the *Nlrc3*$^{-/-}$ mice and PCR analysis for the gene encoding NLRC3 in WT C57BL/6 mice, *Nlrc3*$^{+/-}$ mice and *Nlrc3*$^{-/-}$ mice. The primers P1 (binds a region between Exon 1 and Exon

2) and P2 (binds a region between Exon 3 and Exon 4) were designed for “PCR1” such that it generates a 4804-bp PCR fragment for the WT allele and a 2309-bp fragment for the knockout (KO) allele. However, “PCR1” cannot differentiate heterozygote (HT) and KO mice because the KO 2309-bp fragment outcompeted the WT 4804-bp fragment. Therefore, we designed primers P3 and P4 for use in “PCR2” to amplify a 940-bp fragment from Exon 3 to confirm its presence in WT and HET mice and its absence in KO mice. **d**, Histological scores of the colon tissues in WT and *Nlrc3*$^{-/-}$ mice 80 days after AOM injection **e**, Percentages of mice with dysplasia 80 days after injection of AOM. **f**, Percentages of mice with adenocarcinoma 80 days after injection of AOM. **g**, H&E staining of colon crypts. Scale bar, 100 μm (**g**). Each symbol represents an individual mouse (**b**, **d**). **** P<0.0001; NS, not statistically significant [One-way ANOVA (**b**) or two tailed t-test (**d**)]. Data represent two independent experiments (**b**, **d**–**g**; mean and s.e.m. **b, d**).

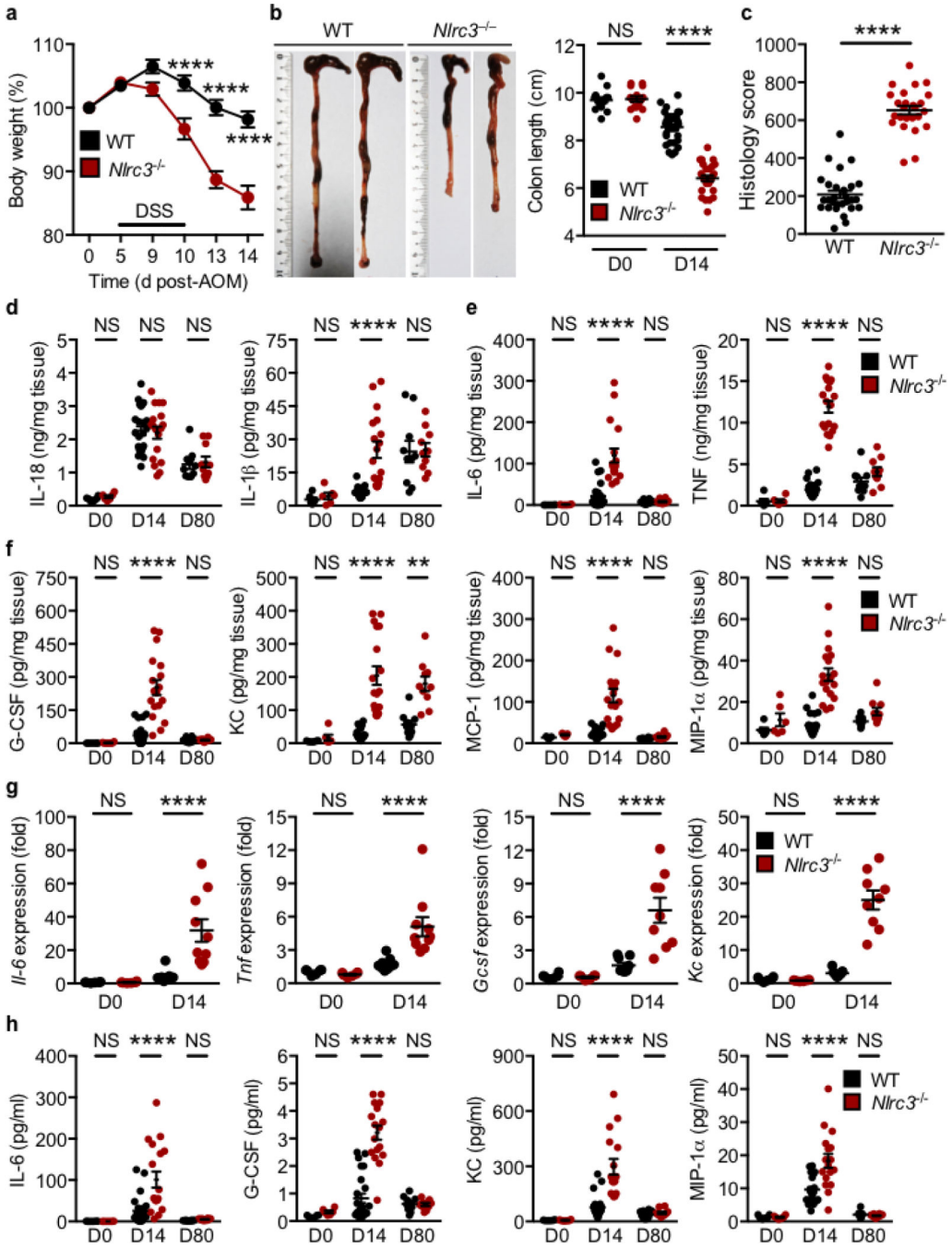

Extended Data Figure 2. NLRC3 dampens intestinal inflammation

a, Body weight change of mice pooled from three independent experiments. **b**, Images of colon and colon length in WT and *Nlrc3*$^{-/-}$ mice 14 days after injection of AOM. **c**, Histological scores 14 days after injection of AOM. **d**, Levels of IL-18 and IL-1β in colon tissues 14 and 80 days after AOM. **e**,**f**, Levels of IL-6, TNF, G-CSF, KC, MCP-1 and MIP-1α in colon tissues 14 and 80 days after AOM. **g**, Relative expression of genes encoding IL-6, TNF, G-CSF and KC in colon tissues of untreated WT and *Nlrc3*$^{-/-}$ mice and in WT and *Nlrc3*$^{-/-}$ mice 14 days after injection of AOM. **h**, Levels of IL-6, G-CSF, KC and

MIP-1α in sera of untreated WT and *Nlrc3*$^{-/-}$ mice and WT and *Nlrc3*$^{-/-}$ mice 14 and 80 days after AOM. Each symbol represents an individual mouse (**b–h**). ** $P<0.01$; **** $P<0.0001$; NS, not statistically significant [One-way ANOVA (**a**) or two tailed *t*-test (**b–h**)]. Data represent three independent experiments (**a–h**; mean and s.e.m. in **a–h**).

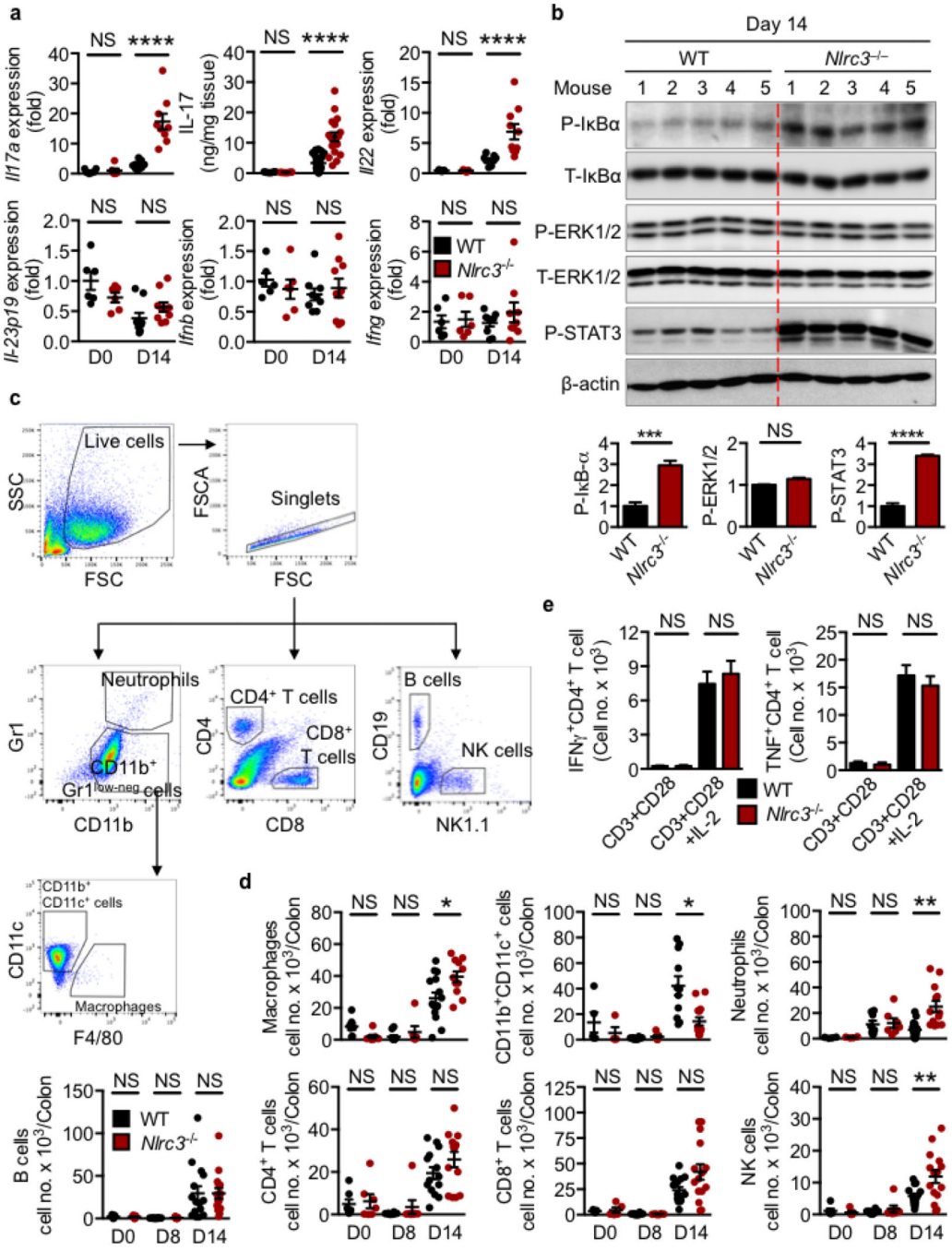

Extended Data Figure 3. NLRC3 governs colorectal tumorigenic susceptibility via inflammatory mediators and immune cells

a, Relative expression of genes encoding IL-17a, levels of the IL-17 protein and relative expression of genes encoding IL-22, IL-23p19, IFN-β and IFN-γ in colon tissues of

untreated WT and *Nlrc3*$^{-/-}$ mice and in WT and *Nlrc3*$^{-/-}$ mice 14 days after AOM injection. **b**, Immunoblot analysis of phosphorylated and total IκBα (P-IκBα and T-IκBα), ERK1 and ERK2 (P-ERK1/2 and T-ERK1/2), phosphorylated STAT3 (P-STAT3), and β-actin (loading control) in colon tissues of WT and *Nlrc3*$^{-/-}$ mice 14 days after injection of AOM (top). The protein band intensity was normalized to the total protein counterpart and/or β-actin, and expressed relative to that of WT controls, set at 1 (bottom). **c**, Gating strategies used to generate data in **d. d**, Number of macrophages, CD11b^{+}CD11c^{+} cells, neutrophils, B cells, CD4^{+} T cells, CD8^{+} T cells and NK cells per colon in WT and *Nlrc3*$^{-/-}$ mice 8 and 14 days after injection of AOM. **e**, Splenocytes from WT and *Nlrc3*$^{-/-}$ mice were stimulated with CD3, CD28 and IL-2, and the intracellular staining was performed for IFN-γ and TNF. * $P<0.05$; ** $P<0.01$; *** $P<0.001$; **** $P<0.0001$; NS, not statistically significant, two tailed *t*-test (**a**, **b**, **d** and **e**). Data pooled from two independent experiments (**a**) or represent one experiment representative of two independent experiments (**b**–**e**; mean and s.e.m. in **a**, **b**, **d** and **e**).

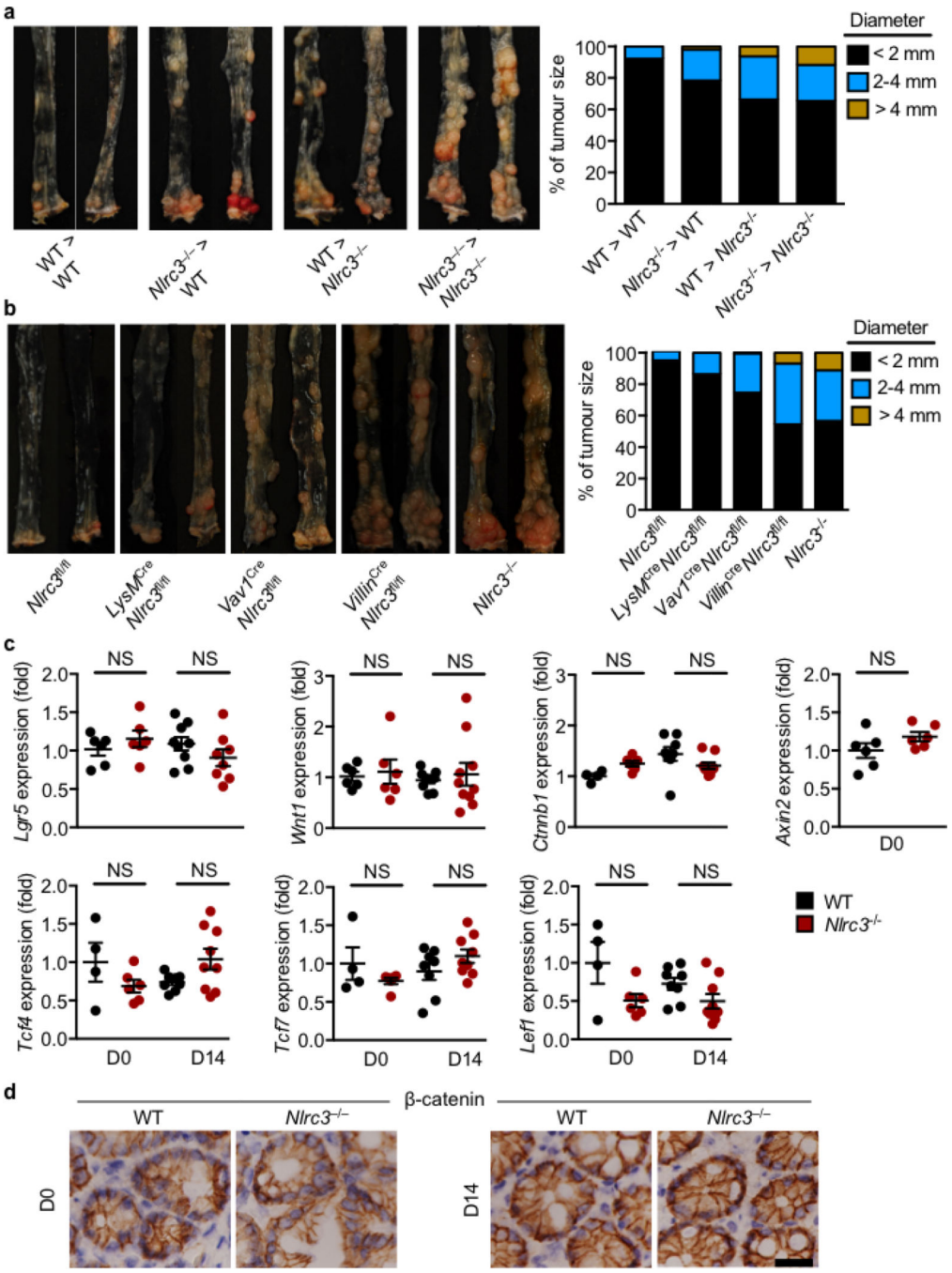

Extended Data Figure 4. The inhibitory effect of NLRC3 is more dominant in intestinal epithelial cells than in haematopoietic cells

a, Colon tumours in bone marrow chimeric mice (1) WT→WT (n=10); (2) *Nlrc3*$^{-/-}$→WT (n=9); (3) WT→*Nlrc3*$^{-/-}$ (n=8); (4) *Nlrc3*$^{-/-}$→*Nlrc3*$^{-/-}$ (n=9) 80 days after injection of AOM (left). Percentages of the tumour size of mice (right). **b**, Colon tumours in littermate *Nlrc3*$^{fl/fl}$ (n=8), *LysM*^{cre}*Nlrc3*$^{fl/fl}$ (n=11), *Vav1*^{cre}*Nlrc3*$^{fl/fl}$ (n=9), *Villin*^{cre}*Nlrc3*$^{fl/fl}$ (n=7) and *Nlrc3*$^{-/-}$ (n=8) mice 80 days after injection of AOM (left). Percentages of the tumour size of mice (right). **c**, Relative expression of genes encoding LGR5, WNT1, β-catenin (Ctnnb1),

Axin2, TCF4, TCF7, and LEF1 in colon tissues of untreated WT and *Nlrc3*$^{-/-}$ mice or in WT and *Nlrc3*$^{-/-}$ mice 14 days after injection of AOM. **d**, Immunohistochemical staining of β-catenin in colon tissues of WT and *Nlrc3*$^{-/-}$ mice. Scale bar, 20 μm (**d**). Each symbol represents one mouse (**c**). NS, not statistically significant (two tailed *t*-test). Data represent two independent experiments (mean and s.e.m. in **c**).

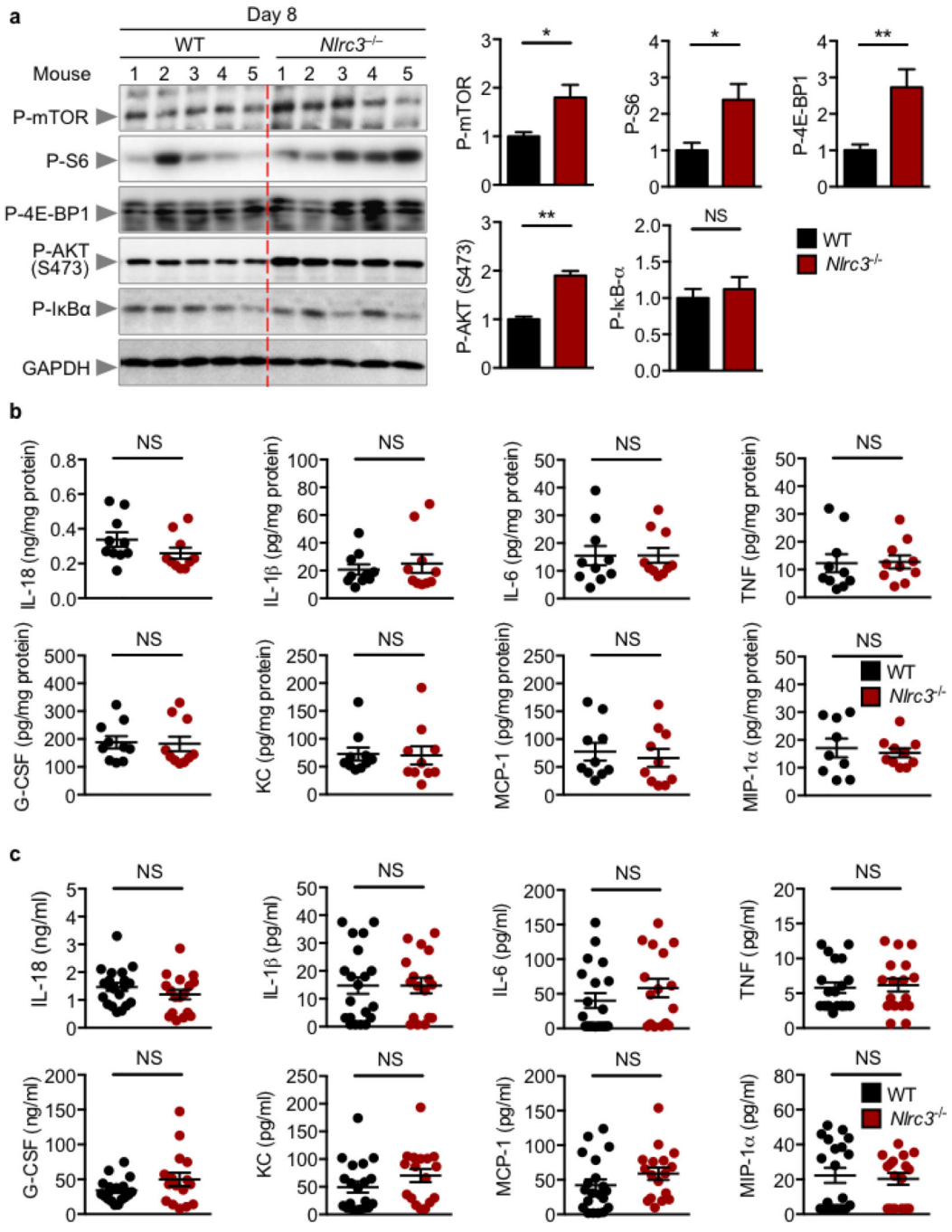

Extended Data Figure 5. Dysregulation of mTOR signalling precedes dysregulation of NF-kB signalling

a, Immunoblot analysis of phosphorylated mTOR (P-mTOR), S6 (P-S6), 4E–BP1 (P-4E–BP1), AKT (P-AKT S473), IκBα (P-IκBα) and GAPDH (loading control) in colon tissues of WT and *Nlrc3*$^{-/-}$ mice 8 days after injection of AOM (left). The protein band intensity was normalized to GAPDH and expressed relative to that of WT controls, set at 1 (right). **b**, Levels of IL-18, IL-1β, IL-6, TNF, G-CSF, KC, MCP-1 and MIP-1α in colon tissues 8 days after injection of AOM. **c**, Levels of IL-18, IL-1β, IL-6, TNF, G-CSF, KC, MCP-1 and MIP-1α in sera. Each symbol represents an individual mouse (**b, c**). * $P<0.05$; ** $P<0.01$; NS, not statistically significant [two tailed *t*-test (**a**–**c**)]. Data represent two independent experiments (mean and s.e.m. in **a**–**c**). For gel source data, see Supplementary Figure 1.

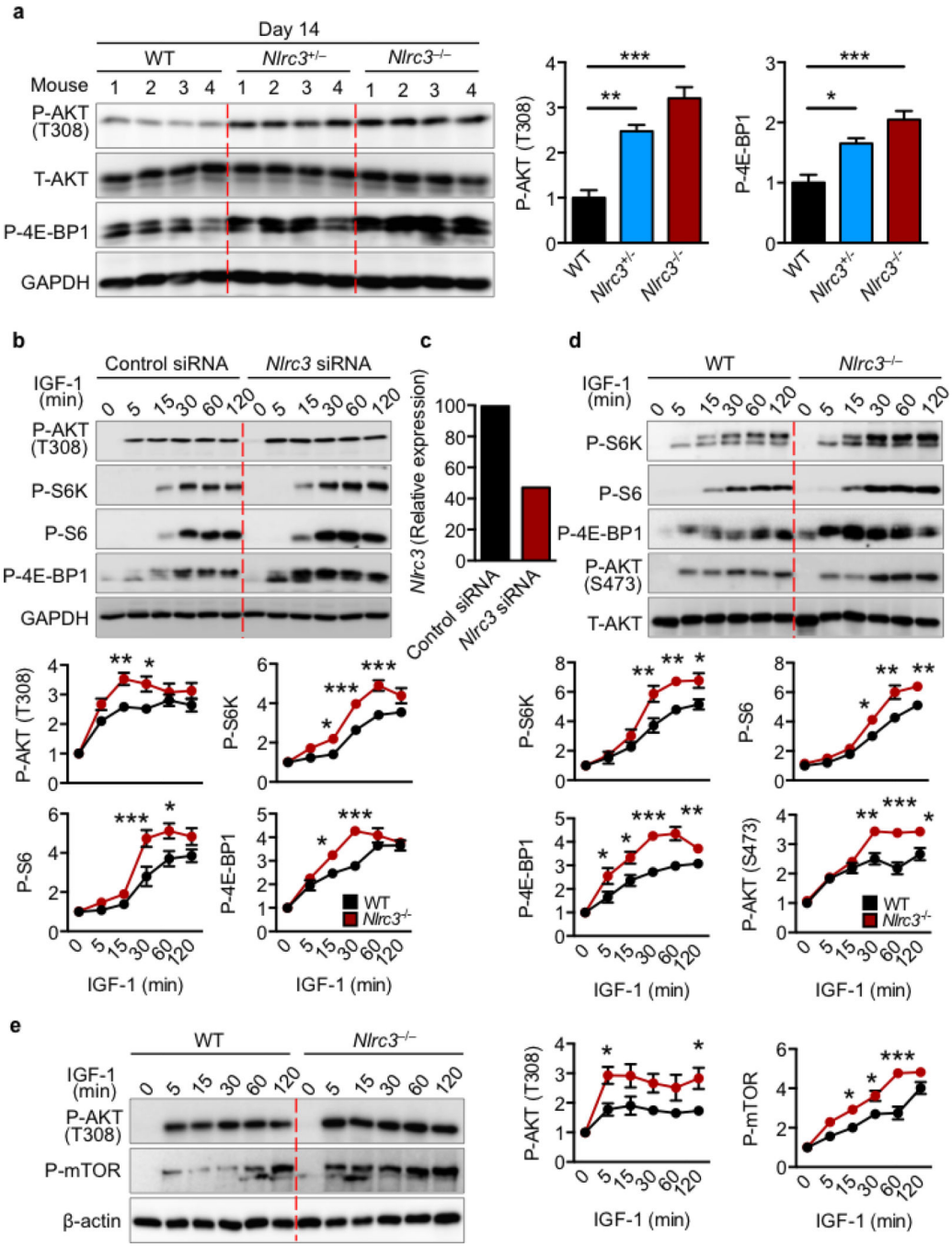

Extended Data Figure 6. NLRC3 regulates mTOR activity

a, Immunoblot analysis of phosphorylated AKT (P-AKT T308), total AKT (T-AKT), phosphorylated 4E–BP1 (P-4E–BP1) and GAPDH (loading control) in colon tissues of WT, *Nlrc3*$^{+/-}$ and *Nlrc3*$^{-/-}$ mice 14 days after injection of AOM (left). The protein band intensity was normalized to the total protein counterpart and/or loading controls, and expressed relative to that of WT controls, set at 1 (right). **b**, Immunoblot analysis of phosphorylated AKT (P-AKT T308), S6K (P-S6K), S6 (P-S6) and 4E–BP1 (P-4E–BP1), and GAPDH (loading control) in WT fibroblasts transfected with a control siRNA or *Nlrc3* siRNA left

untreated or treated with IGF-1 (top). Densitometry analysis as in **a** (bottom). **c**, Relative expression of the gene encoding NLRC3 in WT fibroblasts transfected with a control siRNA or compared with WT fibroblasts transfected with an *Nlrc3* siRNA. **d**, Immunoblotting of phosphorylated S6K (P-S6K), S6 (P-S6), 4E–BP1 (P-4E–BP1), AKT (P-AKT S473), and total AKT (T-AKT) in primary fibroblasts left untreated or treated with IGF-1 (top). Densitometry analysis as in **a** (bottom). **e**, Immunoblotting of phosphorylated AKT (P-AKT T308) and mTOR (P-mTOR) in primary fibroblasts left untreated or treated with IGF-1 (left). Densitometry analysis as in **b** (right). $*P<0.05$; $**P<0.01$; $***P<0.001$ [One-way ANOVA (**a**, **b**, **d** and **e**)]. Data are from one experiment representative of two (**a**, **c**) or four independent experiments (**b**, **d** and **e**; mean and s.e.m. in **a**, **b**, **d** and **e**). For gel source data, see Supplementary Figure 1.

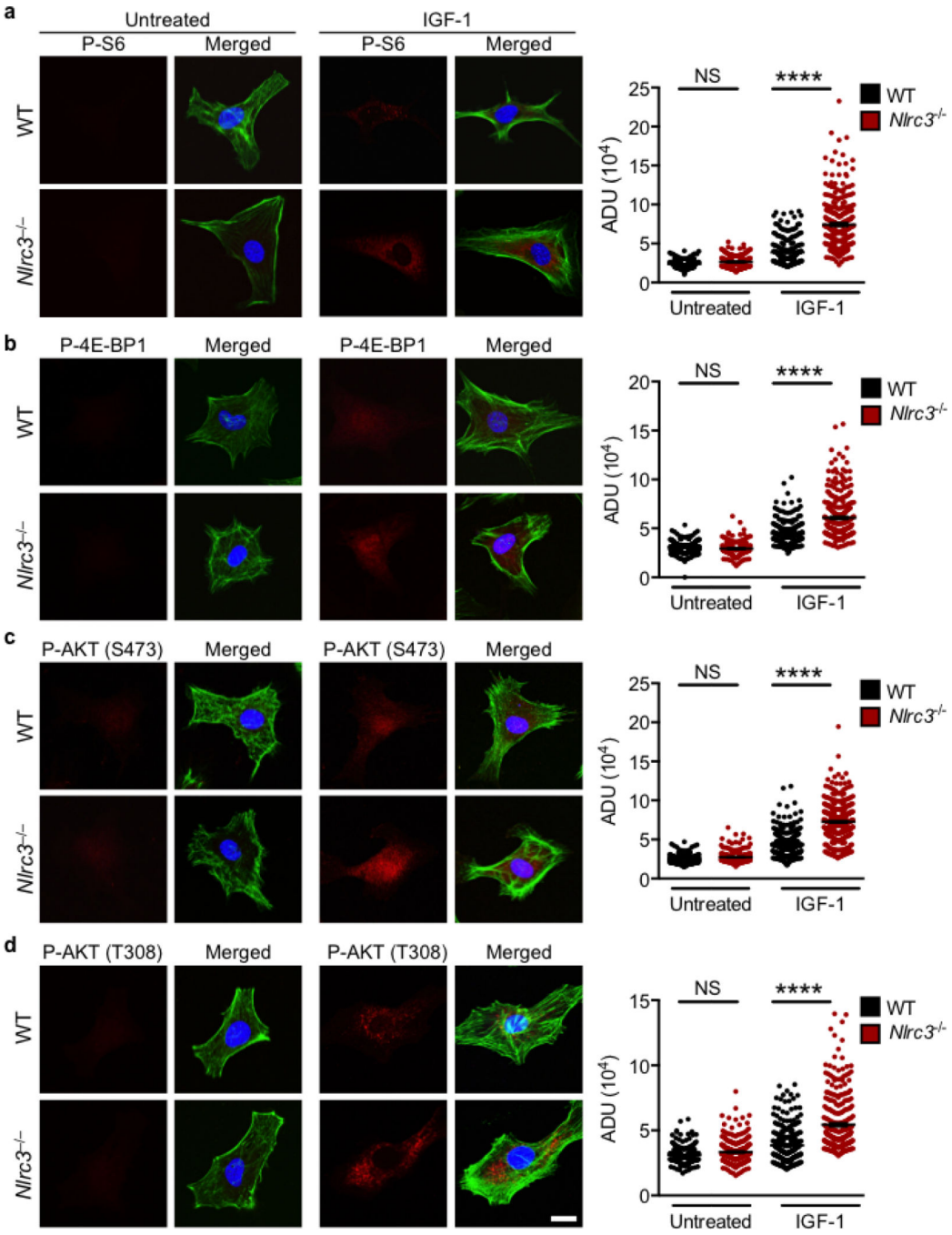

Extended Data Figure 7. NLRC3 regulates mTOR activity in fibroblasts

a–**d**, Immunofluorescence staining of phosphorylated **a**, S6 (P-S6), **b**, 4E–BP1 (P-4E–BP1), **c**, AKT (P-AKT S473), and **d**, AKT (P-AKT T308) in primary fibroblasts left untreated or treated with IGF-1 for 30 min (left). Quantification of the fluorescence intensity (right) in each cell (n=150 or more). Scale bar, 20 μm (**a**–**d**). Each symbol represents an individual cell (**a**–**d**). ADU, average density unit (**a**–**d**). **** P<0.0001; NS, not statistically significant [two tailed t-test (**a**–**d**)]. Data represent one experiment representative of two independent experiments (mean and s.e.m.).

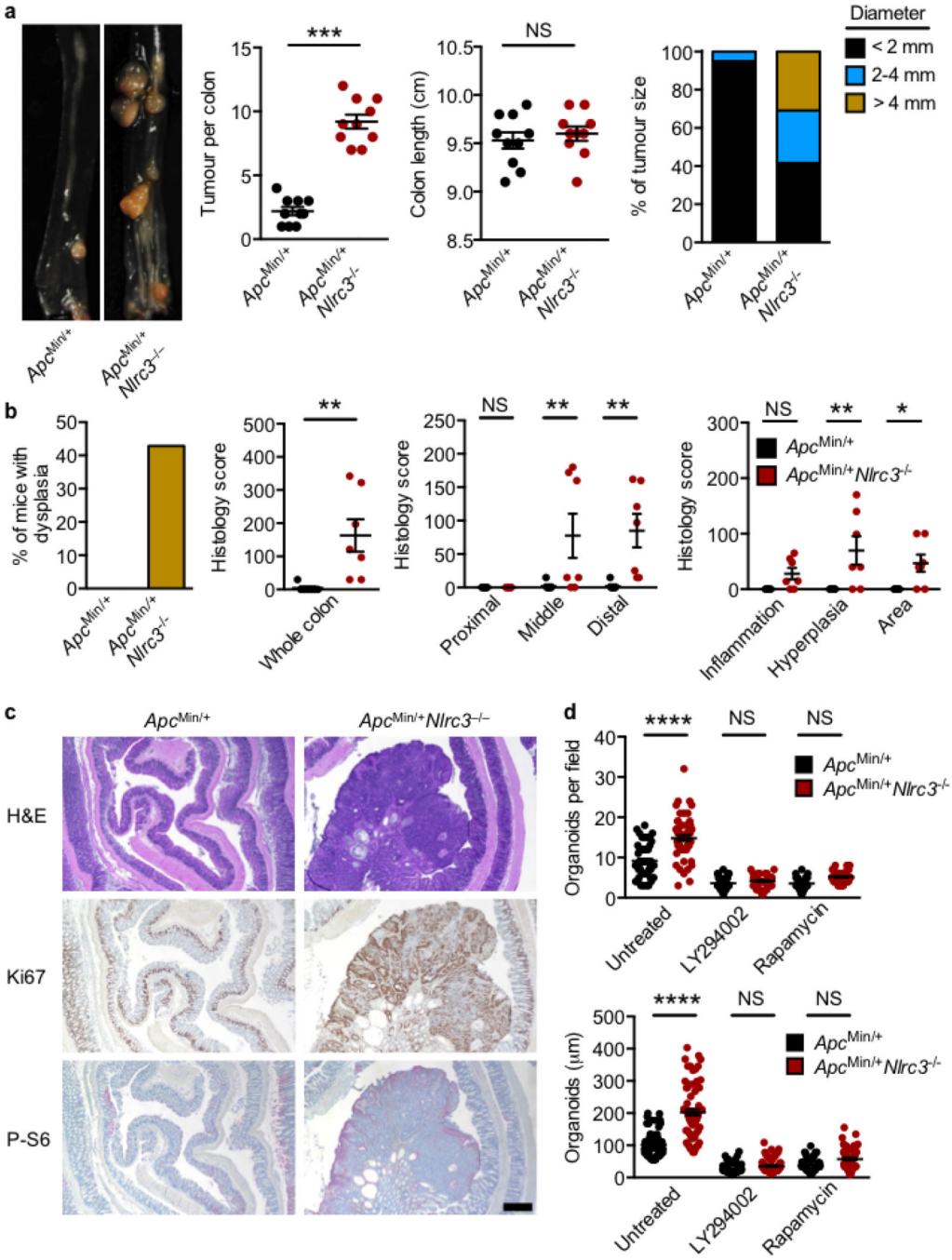

Extended Data Figure 8. NLRC3 prevents colorectal cancer in an *Apc*$^{Min/+}$ model of tumorigenesis

a, Images of colon tumours (left), and tumour number and colon length (middle), and size (right) of 120-days-old littermate *Apc*$^{Min/+}$ and *Apc*$^{Min/+}$*Nlrc3*$^{-/-}$ mice. **b**, Percentages of mice with dysplasia (left), total histology scores (middle) and histology scores of different parts of colon and different parameters (right) of mice in **a. c**, H&E (top), Ki67 (middle) and phosphorylated S6 (P-S6, bottom) staining of colon tumours, **d**, Quantification of the number (top) and size (bottom) of organoids derived from colonic stem cells of *Apc*$^{Min/+}$

and *Apc*$^{Min/+}$*Nlrc3*$^{-/-}$ mice left untreated or treated with LY294002 and rapamycin. Scale bar, 200 μm (**c**). * $P<0.05$; ** $P<0.01$; *** $P<0.001$; **** $P<0.0001$; NS, not statistically significant [two tailed *t*-test (**a**, **b** and **d**)]. Data represent two independent experiments (mean and s.e.m. in **a**, **b** and **d**).

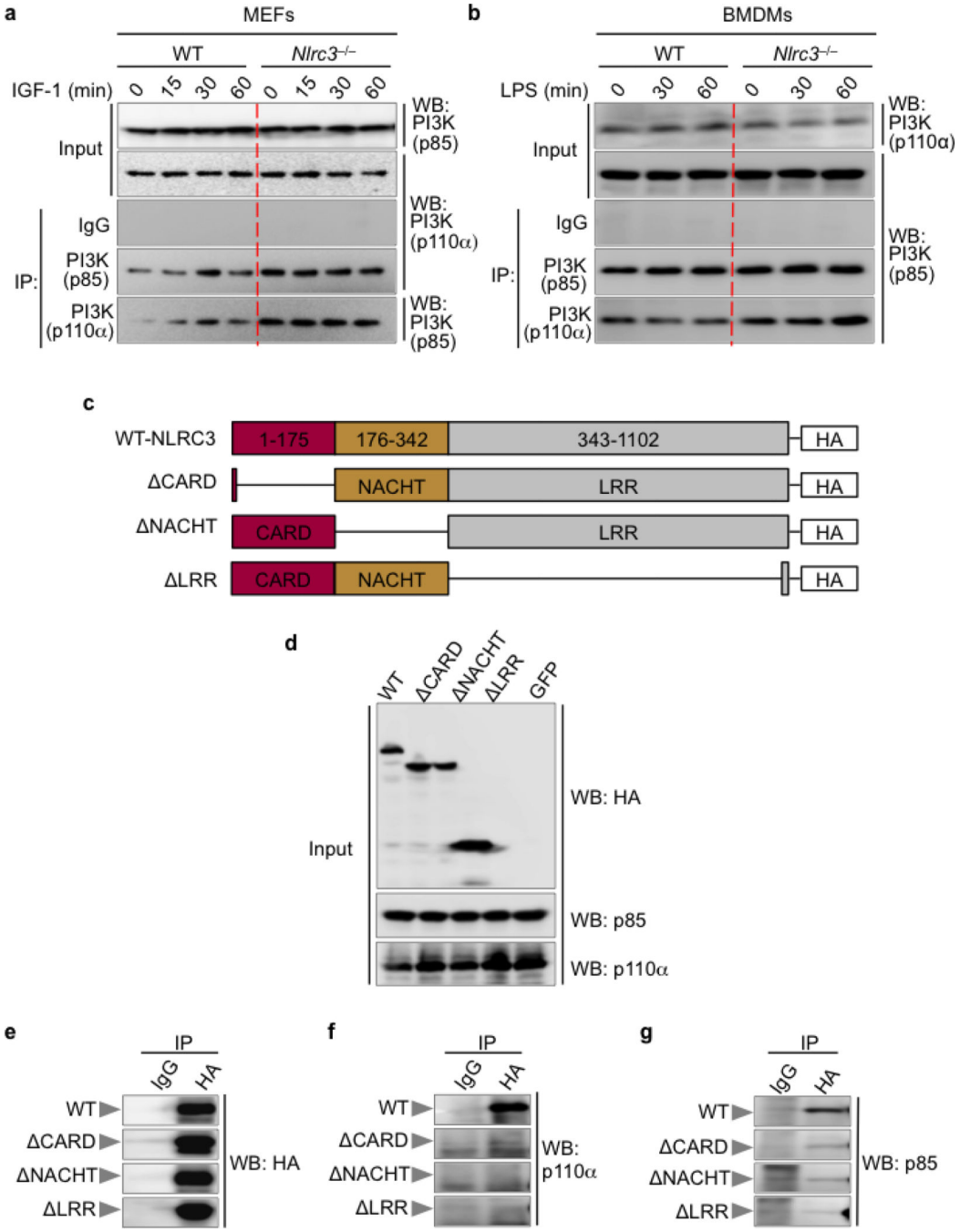

Extended Data Figure 9. NLRC3 disrupts the assembly of the PI3K heterodimeric complex

Immunoprecipitation and comparative analysis of the PI3K signalling complex levels between **a**, WT and *Nlrc3*$^{-/-}$ primary fibroblasts (MEFs) and **b**, bone marrow-derived

macrophages (BMDMs). **c**, Schematic representation of generation of deletion mutants of NLRC3. **d**, Loading inputs for **e**–**g**. **e**, Immunoprecipitation of WT-NLRC3 and its deletion mutants. Immunoblotting analysis of the interaction between NLRC3 and its mutants with **f**, PI3K–p110 subunit and **g**, PI3K–p85. Data represent two independent experiments. For gel source data, see Supplementary Figure 1.

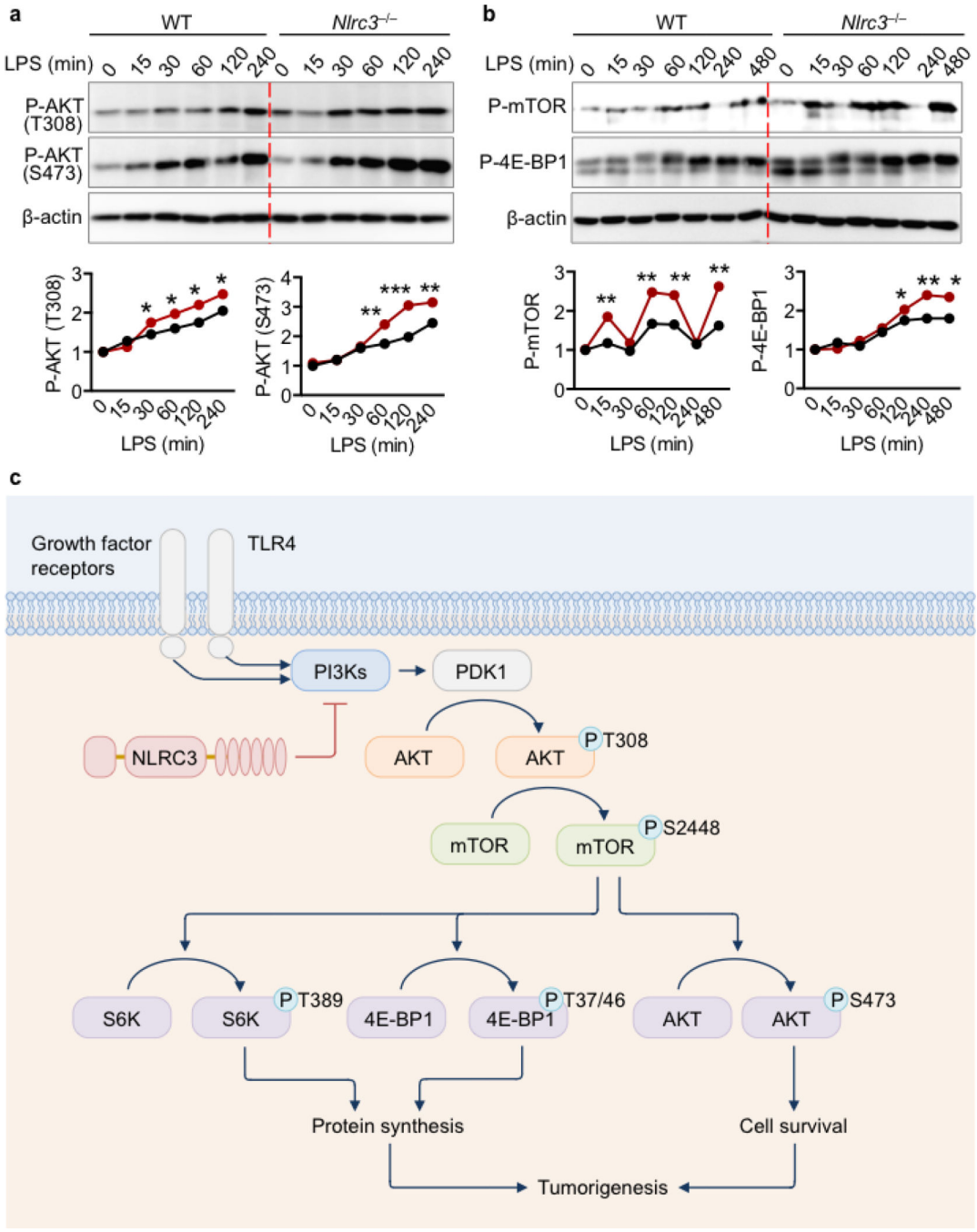

Extended Data Figure 10. NLRC3 negatively regulates TLR4-induced activation of the PI3K–AKT–mTOR pathway

a, Immunoblot analysis of phosphorylated AKT (T308 and S473), total AKT (T-AKT), and β-actin (loading control) in WT and *Nlrc3*$^{-/-}$ bone marrow-derived macrophages (BMDMs) left untreated or treated with LPS (top). The protein band intensity was normalized to β-actin, and expressed relative to that of WT controls, set at 1 (bottom). **b**, Immunoblot analysis of phosphorylated mTOR (P-mTOR), phosphorylated 4E–BP1 (P-4E–BP1), and β-actin (loading control) in WT and *Nlrc3*$^{-/-}$ bone marrow-derived macrophages (BMDMs) left untreated or treated with LPS (top). Densitometry analysis as in **a** (bottom). **c**, A model of the role of NLRC3 in the negative regulation of the PI3K–AKT–mTOR pathway. * $P<0.05$; ** $P<0.01$; *** $P<0.001$ [two tailed *t*-test (**a** and **b**)]. Data are from one experiment representative of four independent experiments (mean and s.e.m. in **a** and **b**). For gel source data, see Supplementary Figure 1.

Supplementary Material

Refer to Web version on PubMed Central for supplementary material.

Acknowledgments

We thank the Transgenic Gene Knockout Shared Resource (St. Jude Children's Research Hospital, SJCRH) for assistance with knockout mouse generation. Images were acquired at the SJCRH Cell & Tissue Imaging Center, which is supported by SJCRH and NCI P30 CA021765-35. Work from our laboratory is supported by the US National Institutes of Health (AI101935, AI124346, AR056296 and CA163507 to T.D.K.), ALSAC (to T.D.K.), and the Cluster of Excellence Inflammation at Interfaces and the SFB877 B9 project (to P.R.). S.M.M is supported by the R.G. Menzies Early Career Fellowship from the National Health and Medical Research Council of Australia.

References

1. Ting JP, Willingham SB, Bergstralh DT. NLRs at the intersection of cell death and immunity. Nature reviews. Immunology. 2008; 8:372–379.
2. Zaki MH, et al. The NLRP3 inflammasome protects against loss of epithelial integrity and mortality during experimental colitis. Immunity. 2010; 32:379–391. [PubMed: 20303296]
3. Zaki MH, Vogel P, Body-Malapel M, Lamkanfi M, Kanneganti TD. IL-18 production downstream of the Nlrp3 inflammasome confers protection against colorectal tumor formation. Journal of immunology. 2010; 185:4912–4920.
4. Allen IC, et al. The NLRP3 inflammasome functions as a negative regulator of tumorigenesis during colitis-associated cancer. The Journal of experimental medicine. 2010; 207:1045–1056. [PubMed: 20385749]
5. Allen IC, et al. NLRP12 suppresses colon inflammation and tumorigenesis through the negative regulation of noncanonical NF-kappaB signaling. Immunity. 2012; 36:742–754. [PubMed: 22503542]
6. Elinav E, et al. NLRP6 inflammasome regulates colonic microbial ecology and risk for colitis. Cell. 2011; 145:745–757. [PubMed: 21565393]
7. Man SM, et al. Critical Role for the DNA Sensor AIM2 in Stem Cell Proliferation and Cancer. Cell. 2015; 162:45–58. [PubMed: 26095253]
8. Wilson JE, et al. Inflammasome-independent role of AIM2 in suppressing colon tumorigenesis via DNA-PK and Akt. Nature medicine. 2015; 21:906–913.
9. Harton JA, Linhoff MW, Zhang J, Ting JP. Cutting edge: CATERPILLER: a large family of mammalian genes containing CARD, pyrin, nucleotide-binding, and leucine-rich repeat domains. Journal of immunology. 2002; 169:4088–4093.
10. Conti BJ, et al. CATERPILLER 16.2 (CLR16.2), a novel NBD/LRR family member that negatively regulates T cell function. The Journal of biological chemistry. 2005; 280:18375–18385. [PubMed: 15705585]

11. Liu R, et al. Expression profile of innate immune receptors, NLRs and AIM2, in human colorectal cancer: correlation with cancer stages and inflammasome components. Oncotarget. 2015; 6:33456–33469. [PubMed: 26378020]
12. Schneider M, et al. The innate immune sensor NLRC3 attenuates Toll-like receptor signaling via modification of the signaling adaptor TRAF6 and transcription factor NF-kappaB. Nature immunology. 2012; 13:823–831. [PubMed: 22863753]
13. Zhang L, et al. NLRC3, a member of the NLR family of proteins, is a negative regulator of innate immune signaling induced by the DNA sensor STING. Immunity. 2014; 40:329–341. [PubMed: 24560620]
14. Man SM, Kanneganti TD. Converging roles of caspases in inflammasome activation, cell death and innate immunity. Nature reviews. Immunology. 2016; 16:7–21.
15. Shimobayashi M, Hall MN. Making new contacts: the mTOR network in metabolism and signalling crosstalk. Nature reviews. Molecular cell biology. 2014; 15:155–162. [PubMed: 24556838]
16. Alessi DR, et al. Characterization of a 3-phosphoinositide-dependent protein kinase which phosphorylates and activates protein kinase Balpha. Current biology : CB. 1997; 7:261–269. [PubMed: 9094314]
17. Stephens L, et al. Protein kinase B kinases that mediate phosphatidylinositol 3,4,5-trisphosphate-dependent activation of protein kinase B. Science. 1998; 279:710–714. [PubMed: 9445477]
18. Stokoe D, et al. Dual role of phosphatidylinositol-3,4,5-trisphosphate in the activation of protein kinase B. Science. 1997; 277:567–570. [PubMed: 9228007]
19. Sancak Y, et al. Ragulator-Rag complex targets mTORC1 to the lysosomal surface and is necessary for its activation by amino acids. Cell. 2010; 141:290–303. [PubMed: 20381137]
20. Zoncu R, et al. mTORC1 senses lysosomal amino acids through an inside-out mechanism that requires the vacuolar H(+)-ATPase. Science. 2011; 334:678–683. [PubMed: 22053050]
21. Monick MM, et al. Lipopolysaccharide activates Akt in human alveolar macrophages resulting in nuclear accumulation and transcriptional activity of beta-catenin. Journal of immunology. 2001; 166:4713–4720.
22. Jones BW, Heldwein KA, Means TK, Saukkonen JJ, Fenton MJ. Differential roles of Toll-like receptors in the elicitation of proinflammatory responses by macrophages. Annals of the rheumatic diseases. 2001; 60(Suppl 3):6–12. [PubMed: 11114274]
23. Ojaniemi M, et al. Phosphatidylinositol 3-kinase is involved in Toll-like receptor 4-mediated cytokine expression in mouse macrophages. European journal of immunology. 2003; 33:597–605. [PubMed: 12616480]
24. Laudien M, et al. Molecular signatures of a disturbed nasal barrier function in the primary tissue of Wegener's granulomatosis. Mucosal immunology. 2011; 4:564–573. [PubMed: 21412229]
25. Shiau CE, Monk KR, Joo W, Talbot WS. An anti-inflammatory NOD-like receptor is required for microglia development. Cell reports. 2013; 5:1342–1352. [PubMed: 24316075]

References

26. Pelletier S, Gingras S, Green DR. Mouse genome engineering via CRISPR-Cas9 for study of immune function. Immunity. 2015; 42:18–27. [PubMed: 25607456]
27. Bae S, Park J, Kim JS. Cas-OFFinder: a fast and versatile algorithm that searches for potential off-target sites of Cas9 RNA-guided endonucleases. Bioinformatics. 2014; 30:1473–1475. [PubMed: 24463181]
28. Zhu Q, et al. Cutting edge: STING mediates protection against colorectal tumorigenesis by governing the magnitude of intestinal inflammation. Journal of immunology. 2014; 193:4779–4782.
29. Man SM, et al. The transcription factor IRF1 and guanylate-binding proteins target activation of the AIM2 inflammasome by *Francisella* infection. Nature immunology. 2015; 16:467–475. [PubMed: 25774715]
30. Boussemart L, et al. eIF4F is a nexus of resistance to anti-BRAF and anti-MEK cancer therapies. Nature. 2014; 513:105–109. [PubMed: 25079330]

31. Karki R, et al. Concerted Activation of the AIM2 and NLRP3 Inflammasomes Orchestrates Host Protection against *Aspergillus* Infection. Cell host & microbe. 2015; 17:357–368. [PubMed: 25704009]

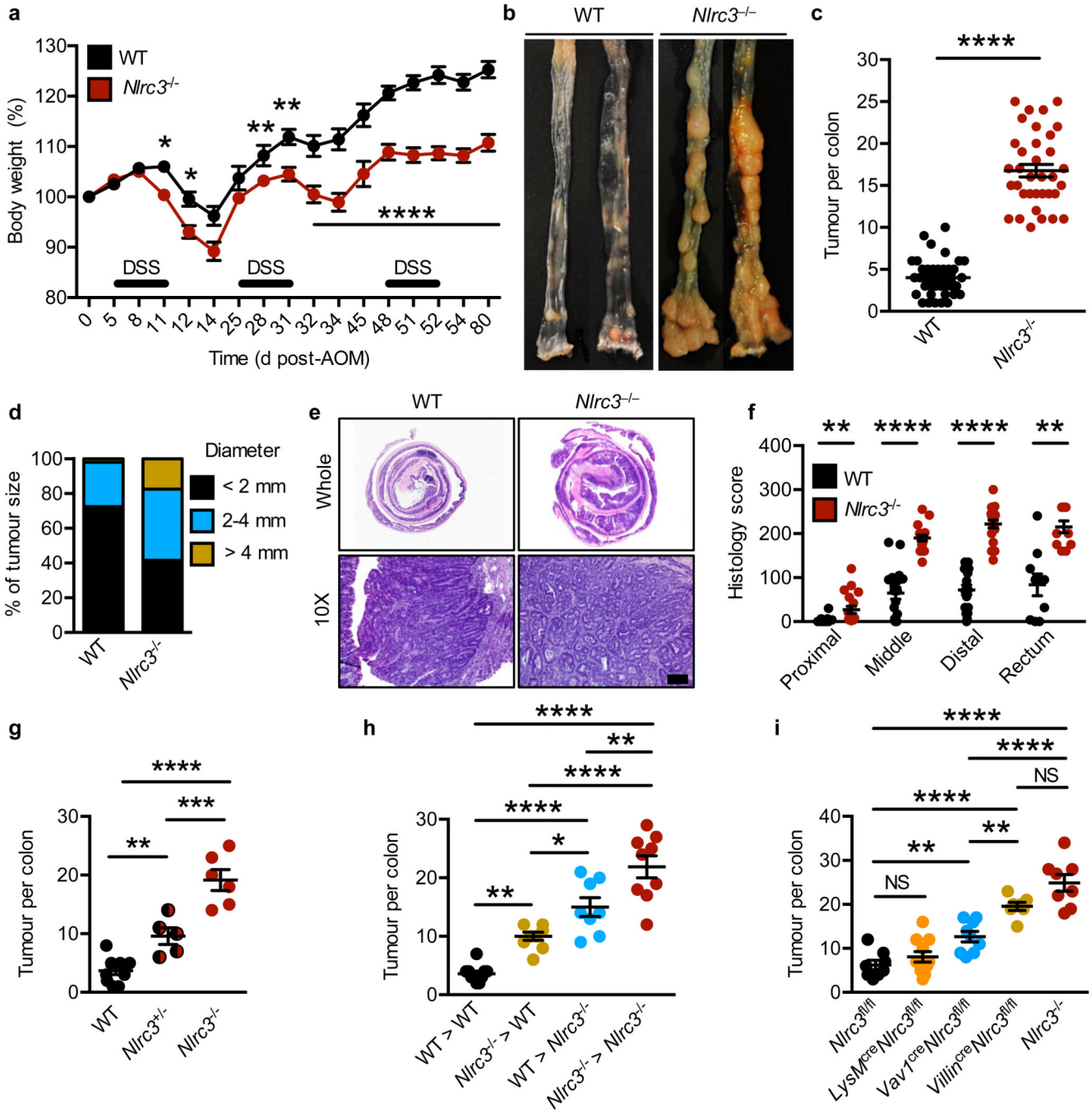

Figure 1. NLRC3 prevents colorectal tumorigenesis

a, Body weight change during AOM-DSS treatment. **b**, Colon tumours in mice 80 days after injection of AOM. **c**, Number and **d**, size of colon tumours in WT (n=37) and *Nlrc3*$^{-/-}$ (n=35) mice. **e**, H&E staining and **f**, histological scores as in b. **g**, Number of colon tumours in littermate WT (n=10), *Nlrc3*$^{+/-}$ (n=5) and *Nlrc3*$^{-/-}$ (n=6) mice. **h**, Number of colon tumours in bone marrow chimera mice treated as in b. WT→WT (n=10); *Nlrc3*$^{-/-}$→WT (n=9); WT→*Nlrc3*$^{-/-}$ (n=8); and *Nlrc3*$^{-/-}$→*Nlrc3*$^{-/-}$ (n=9). **i**, Number of colon tumours in littermate *Nlrc3*$^{fl/fl}$ (n=8), *LysM*^{cre}*Nlrc3*$^{fl/fl}$ (n=11), *Vav1*^{cre}*Nlrc3*$^{fl/fl}$ (n=9), *Villin*^{cre}*Nlrc3*$^{fl/fl}$

(n=7) and *Nlrc3*$^{-/-}$ (n=8) mice treated as in b. Scale bar, 200 μm (**e**). Each symbol represents an individual mouse (**c**, **f**–**i**). **P*<0.05; ***P*<0.01; ****P*<0.001; *****P*<0.0001; NS, not statistically significant [one-way ANOVA (**a**,**g**–**i**) or two tailed *t*-test (**c**,**f**)]. Data are from three independent experiments (**a**–**f**) and two independent experiments (**g**–**i**; mean and s.e.m. in **a**,**c**, **f**–**i**).

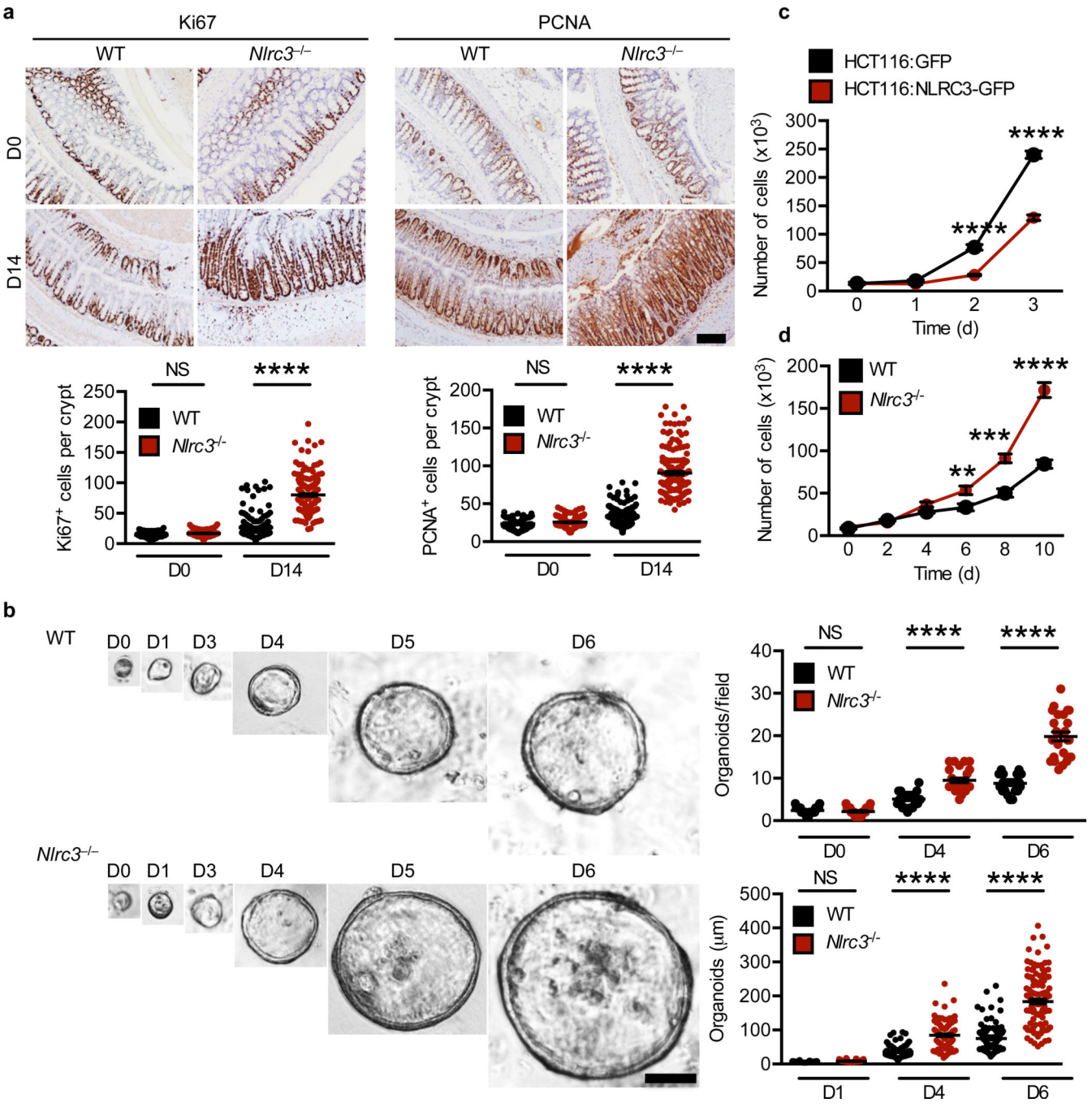

Figure 2. NLRC3 suppresses overt proliferation

a, Images and quantification of the number of Ki67$^+$ (left) and PCNA$^+$ (right) cells in each crypt of WT (day 0, n=5; day 14, n=8) and *Nlrc3*$^{-/-}$ (day 0, n=5; day 14, n=8) mice. **b**, Images (left) and quantification of the number (top right) and size (bottom right) of mouse intestinal organoids. **c**, Proliferation of the HCT116 cell line. **d**, Proliferation of primary mouse fibroblasts. At least 25 crypts were counted in each animal (**a**). Scale bars, 200 μm (**a**), 50 μm (**b**). Each symbol represents one crypt (**a**) or one organoid (**b**). $^{**}P<0.01$; $^{***}P<0.001$; $^{****}P<0.0001$; NS, no statistical significance [two tailed *t*-test (**a–d**)]. Data are

from one experiment representative of two (**a**, **b**) or three independent experiments (**c**, **d**; mean and s.e.m. in **a**–**d**).

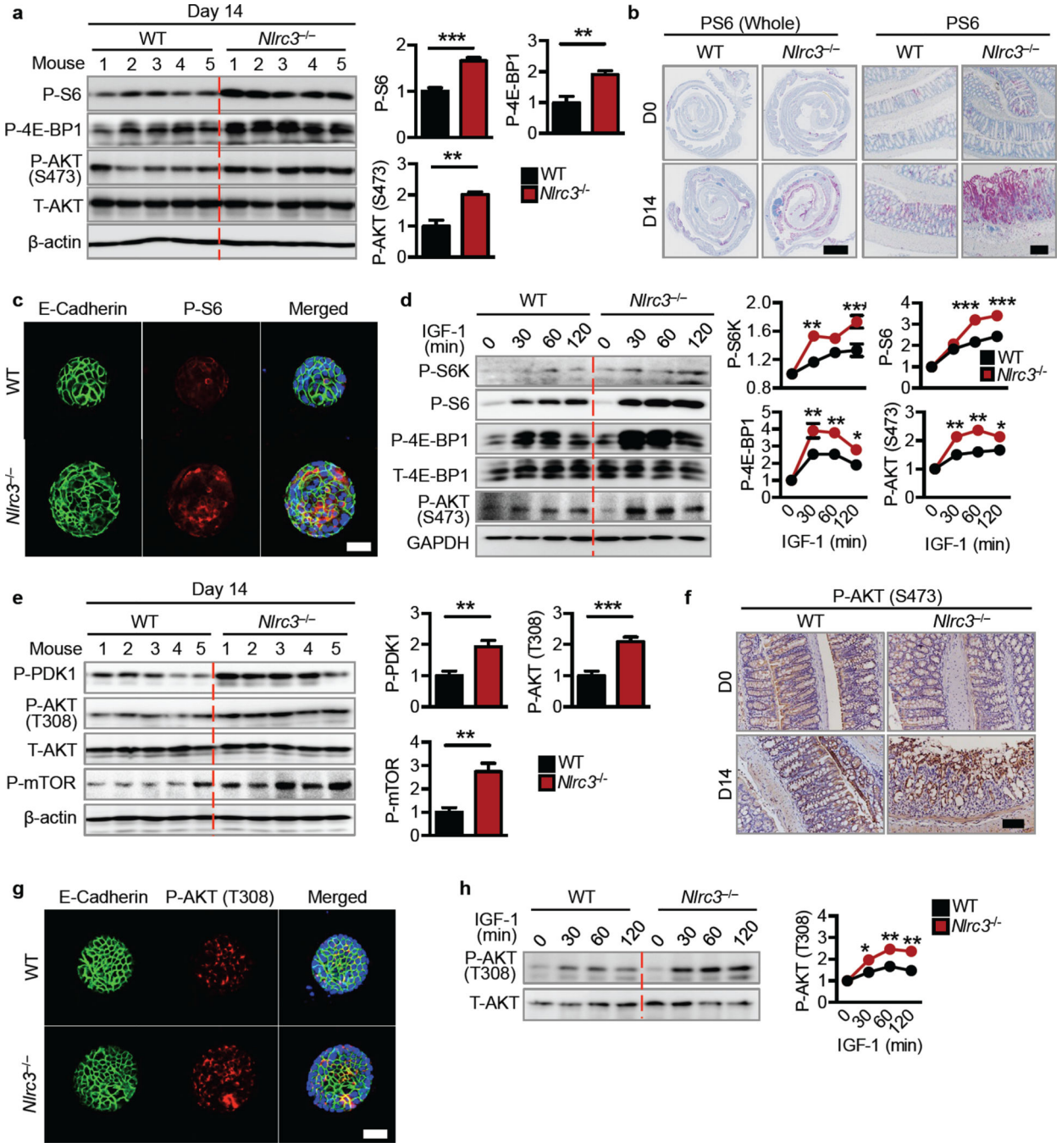

Figure 3. NLRC3 controls mTOR signalling pathways

a, Immunoblot of mouse colon tissues and densitometric quantification. **b**, Immunohistochemical staining of mouse colon tissues. **c**, Immunofluorescence staining of mouse intestinal organoids after 7 days of culture. **d**, Immunoblot of organoids treated with IGF-1 and densitometric quantification. **e**, Immunoblot of colon tissues of mice and densitometric quantification. **f**, Immunohistochemical staining of colon tissues of mice. **g**, Immunofluorescence staining of mouse intestinal organoids after 7 days of culture. **h**, Immunoblot of organoids treated with IGF-1 and densitometric quantification. Scale bars,

2,500 μm (**b**, whole colon, left), 200 μm (**b**, magnified, right), 50 μm (**c, f, g**). **P*<0.05 ***P*<0.01; ****P*<0.001; [two tailed *t*-test (**a** and **e**); one-way ANOVA (**d** and **h**)]. Data are from one experiment representative of two (**a**–**c**, **e**–**g**) or three independent experiments (**d**, **h**; mean and s.e.m. in **a**, **d**, **e** and **h**). For gel source data, see Supplementary Figure 1.

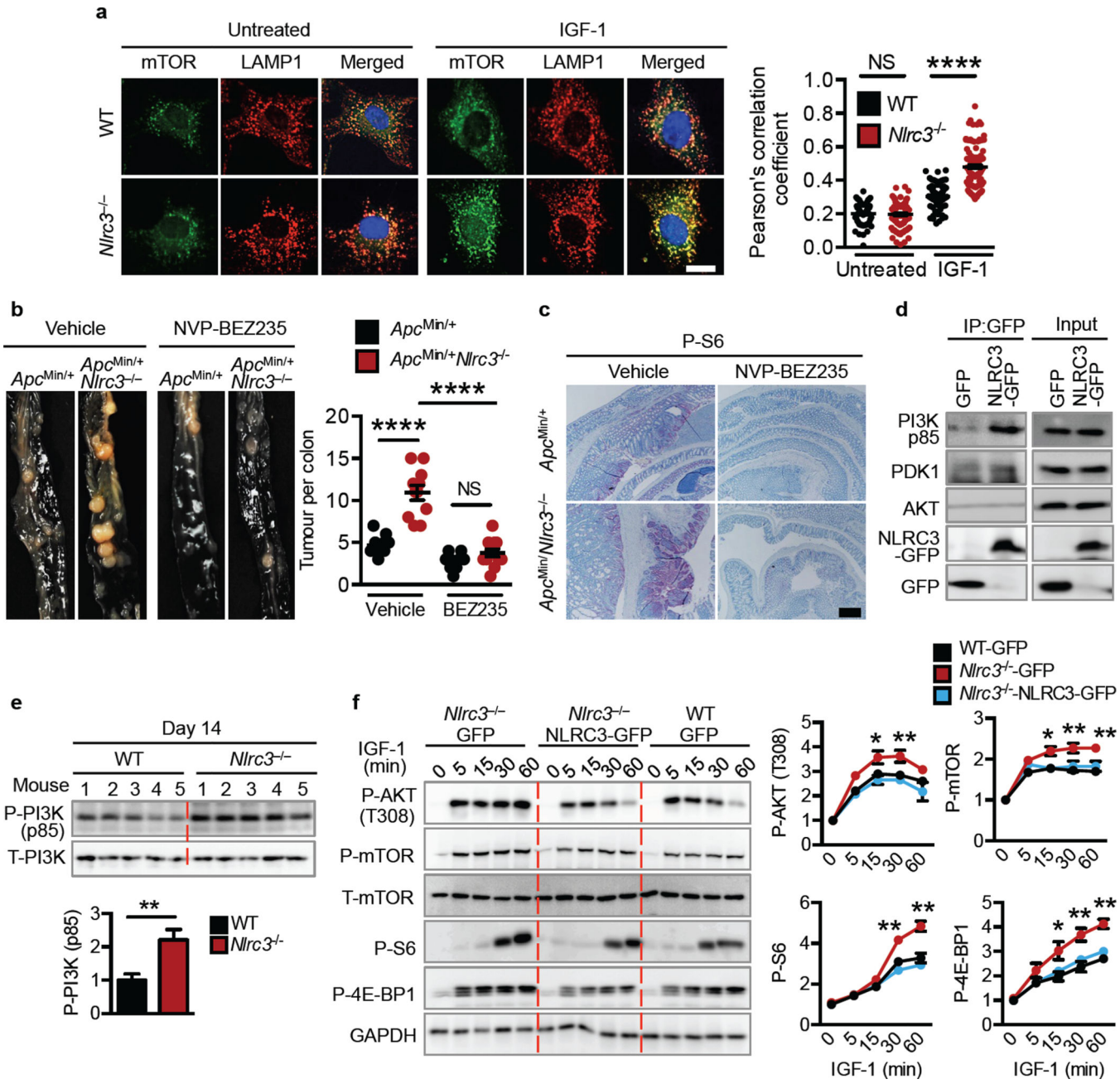

Figure 4. NLRC3 regulates upstream signalling molecules within the PI3K–AKT–mTOR pathway

a, Immunofluorescence staining of primary fibroblasts and frequency of co-localisation between mTOR and LAMP1 (n=>150). **b**, Images and quantification of colon tumours in littermate $Apc^{Min/+}$ and $Apc^{Min/+}Nlrc3^{-/-}$ mice 40 days after treatment with vehicle or NVP-BEZ235. **c**, Immunohistochemical staining of colon tissues from mice treated as in b. **d**, Immunoprecipitation of the GFP tag in 239T cells transfected with a plasmid encoding GFP alone or NLRC3-GFP. **e**, Immunoblot of mouse colon tissues and densitometric quantification. **f**, Immunoblot of primary mouse fibroblasts transduced with a retroviral vector encoding GFP or NLRC3-GFP, with or without stimulation with IGF-1, and

densitometric quantification. Scale bar, 10 μm (**a**), 200 μm (**c**). **P*<0.05 ***P*<0.01; *****P*<0.0001; NS, no statistical significance [two tailed *t*-test (**e**) and one-way ANOVA (**a**, **b** and **f**)]. Data are from one experiment representative of two (**a**–**c** and **e**) or three (**d** and **f** independent experiments (mean and s.e.m. in **a**, **b**, **e** and **f**). For gel source data, see Supplementary Figure 1.